

Matthieu Lengaigne · Eric Guilyardi  
Jean-Philippe Boulanger · Christophe Menkes  
Pascale Delecluse · Pete Inness · Jeff Cole · Julia Slingo

## Triggering of El Niño by westerly wind events in a coupled general circulation model

Received: 2 September 2003 / Accepted: 7 May 2004 / Published online: 4 August 2004  
© Springer-Verlag 2004

**Abstract** Two ten-members ensemble experiments using a coupled ocean-atmosphere general circulation model are performed to study the dynamical response to a strong westerly wind event (WWE) when the tropical Pacific has initial conditions favourable to the development of a warm event. In the reference ensemble (CREF), no wind perturbation is introduced, whereas a strong westerly wind event anomaly is introduced in boreal winter over the western Pacific in the perturbed ensemble (CWWE). Our results demonstrate that an intense WWE is capable of establishing the conditions under which a strong El Niño event can occur. First, it generates a strong downwelling Kelvin wave that generates a positive sea surface temperature (SST) anomaly in the central-eastern Pacific amplified through a coupled ocean-atmosphere interaction. This anomaly can be as large as 2.5°C 60 days after the WWE. Secondly, this WWE also initiates an eastward displacement of the warm-pool that promotes the occurrence of subsequent WWEs in the following months. These events reinforce the initial warming through the generation of additional Kelvin waves and generate intense surface jets at the eastern edge of the warm-pool that act to further shift warm waters eastward. The use of a ten-members ensemble however reveals substantial differences in the coupled response to a WWE. Whereas four members of CWWE ensemble develop into intense El

Niño warming as described above, four others display a moderate warming and two remains in neutral conditions. This diversity between the members appears to be due to the internal atmospheric variability during and following the inserted WWE. In the four moderate warm cases, the warm-pool is initially shifted eastward following the inserted WWE, but the subsequent weak WWE activity (when compared to the strong warming cases) prevents to further shift the warm-pool eastwards. The seasonal strengthening of trade winds in June–July can therefore act to shift warm waters back into the western Pacific, reducing the central-eastern Pacific warming. This strong sensitivity of the coupled response to WWEs may therefore limit the predictability of El Niño events, as the high frequency wind variability over the warm pool region remains largely unpredictable even at short time lead.

### 1 Introduction

While early studies (Wyrтки 1975) considered ENSO (El Niño/southern oscillation) events individually, the development of simple and intermediate coupled models led to a new theory, known as the delayed action oscillator, where ENSO is investigated as a cyclic quasi-periodic self-sustained phenomenon (see Neelin et al. 1998, for a review). Numerous observational (Zhang and Rothstein 2000; Larkin and Harrison 2002) and coupled general circulation models (GCM) studies (Schneider et al. 1997; Knutson et al. 1997) have attempted to confirm this theory. Some observational studies have indeed demonstrated that the termination of El Niño is often consistent with the cyclic nature of delayed oscillator physics (Mantua and Battisti 1994; Boulanger and Menkes 1999), but other studies (Kessler 2002; Guilyardi et al. 2003) suggest that each El Niño warm event is relatively independent.

In fact, the ENSO phenomenon observed during the past two decades rather appears as a moderately

---

M. Lengaigne (✉) · J.-P. Boulanger · C. Menkes  
Laboratoire d'Océanographie  
Dynamique et de Climatologie (CNRS/UPMC/IRD),  
Université Pierre et Marie Curie, Paris, France  
E-mail: lengaign@lodyc.jussieu.fr  
Tel.: +33-1-44277161  
Fax: +33-1-44277159

E. Guilyardi · P. Inness · J. Cole · J. Slingo  
Center for Global Atmospheric Modelling,  
Department of Meteorology,  
University of Reading, UK

P. Delecluse  
Laboratoire des Sciences du Climat et de l'Environnement,  
(CEA/CNRS), Gif-sur-Yvette, France

damped phenomenon, excited by sub-seasonal atmospheric forcing (Penland and Sardeshmukh 1995; Thompson and Battisti 2001; Fedorov et al. 2003). The atmospheric events that lead to a triggering of El Niño seem usually to occur in the first months of the year, but the processes that lead to El Niño onset and to the modulation of its intensity are still being debated. One of the most common hypotheses is the impact of intraseasonal wind activity over the western Pacific, often referred as westerly wind events (WWEs). Although the possible causes of WWEs are still unclear, the favoured candidate is the active phase of the Madden–Julian oscillation, or MJO (Madden and Julian 1994). Otherwise, WWEs of strong to exceptional intensity, such as those during the 1997/1998 El Niño, are often a combination of various factors, including the MJO, cold surges from mid latitudes, tropical cyclones and other mesoscale phenomena (Yu and Rienecker 1998; Lengaigne et al. 2004). They occur preferentially in boreal fall–winter season and are sometimes isolated events or sometimes embedded in a sequence of episodes.

Various studies have analysed the dynamical response of the ocean to WWEs using observations (McPhaden et al. 1988; Vecchi and Harrison 2000; McPhaden 2002) or models (Giese and Harrison 1991; Boulanger et al. 2001; Belamari et al. 2003). All these studies demonstrated that WWEs trigger an eastern equatorial Pacific warming, associated with the generation of equatorial downwelling Kelvin waves. It has therefore been further hypothesised that air–sea interactions involving WWEs and oceanic Kelvin waves could be instrumental to the fast growth of El Niño events and the modulation of ENSO characteristics (Moore and Kleeman 2000; McPhaden and Yu 1999). However there have only been a few studies of the effects of WWEs on the *coupled* ocean–atmosphere system. Those with simple models suggest that WWEs can trigger an El Niño event (Perigaud and Cassou 2000; Fedorov 2002; Boulanger et al. 2003) but their simple models physics may not allow a realistic representation of all the coupled interactions that lead to El Niño onset. Nonlinear effects, not described in many simple models, may have an essential role by further amplifying the warming (Kessler and Kleeman 2000). In particular, coupled processes that occur over the warm-pool following a WWE have been suggested as important features of El Niño onset and growth rate (Kessler and McPhaden 1995; Picaut et al. 1996) but are not represented in most simple models parameterisations.

In two recent papers (Lengaigne et al. 2002, 2003a), the potential role of such warm-pool coupled processes has been highlighted through sensitivity studies with both forced oceanic and atmospheric GCMs. In the first paper, the effect of a strong WWE on the evolution of the tropical Pacific Ocean was explored with a series of simulations using an ocean GCM (OGCM). Then, in a second study, the atmospheric response to the SST changes generated by the WWE was investigated using an atmospheric GCM (AGCM) forced with the SST

anomalies from the ocean-only experiments. By its design, this two-stage procedure simplifies the analysis of the oceanic and atmospheric physical mechanisms involved in the response of the coupled system. By using this ‘decoupled’ method, Lengaigne et al. (2002, 2003a) have demonstrated that a strong WWE can induce a rapid eastward shift of the warm waters through a non-linear mechanism involving the thermohaline front at the eastern edge of the warm pool and the wind forcing. This leads to a further eastward shift of convection that promotes the occurrence of subsequent WWEs to which the ocean is likely to respond further. However, this strategy using forced GCMs prevents the study of the ocean–atmosphere response beyond 3 months following the WWE since coupled processes will surely come into play. As a third phase, the complete study of such complex coupled interactions and their impact on the onset of El Niño and its further development requires the use of a fully coupled GCM (CGCM).

The aim of this paper is therefore to investigate the potential role of WWEs in the onset and development phase of an El Niño event in a fully coupled context. The model used in this study is a recent coupled ocean–atmosphere general circulation model (HadOPA) in which the Hadley Centre atmosphere model (HadAM3) is coupled to the IPSL/LODYC ocean model (OPA). This model is shown to reproduce the tropical Pacific mean state and its mean seasonal cycle with some fidelity. Moreover, the model has a relatively realistic warm-pool representation and is able to generate westerly wind events (WWEs) over the Pacific warm waters through internal dynamics, both features considered essential for the study of the coupled ocean–atmosphere response to WWEs. In this study, a strong WWE is artificially introduced over the western Pacific in the CGCM and the coupled response to this initial disturbance is studied using an ensemble of simulations. The paper is organised as follows. Section 2 includes a brief description of the HadOPA model and a validation of the tropical Pacific. Section 3 is devoted to the experimental strategy and to the ensemble results. In Sect. 4, the response that follows a strong WWE is given in detail for three individual members that are representative of the ensemble, but in which El Niño evolved very differently. Section 5 focuses on the main coupled mechanisms that develop following a strong WWE, and finally, a summary of the results and a discussion of their implications with regard to the ENSO and its predictability are given in Sect. 6.

---

## 2 Coupled model description and validation

### 2.1 The HadOPA coupled model

The coupled GCM used for this study combined the OPA ocean model with the HadAM3 atmospheric model and is called HadOPA (see documentation at [http://www.met.rdg.ac.uk/~ericg/hadop\\_a\\_project.html](http://www.met.rdg.ac.uk/~ericg/hadop_a_project.html)).

Brief description of these models and the coupling procedure are given below.

The OGCM used in this study is the OPA model (Madec et al. 1998, see documentation at <http://www.lodyc.jussieu.fr/opa/>) in its global configuration, known as ORCA2. The horizontal mesh is based on a  $2^\circ$  by  $2^\circ$  Mercator grid (i.e., the same zonal and meridional grid spacing). However, a local transformation is applied to the model grid in the tropics to refine the meridional resolution to up to  $0.5^\circ$  at the equator. The model has 31 levels with a spacing of 10 m in the upper 150 m, increasing to 500 m in the deep ocean. The model uses a free surface formulation (Roulet and Madec 2000). Vertical eddy viscosity and diffusivity coefficients are computed from a 1.5 turbulent closure scheme (Blanke and Delecluse 1993) allowing an explicit formulation of the mixed layer as well as a minimum diffusion in the thermocline. Horizontal viscosity is of Laplacian type and lateral diffusivity is “quasi-pure” isopycnal as described in Guilyardi et al. (2001). There is no interactive sea-ice model in this configuration: sea-ice cover is relaxed towards observed monthly climatology.

This OGCM has been extensively validated in uncoupled mode in the tropics where it closely matches the observations (Vialard et al. 2001; Lengaigne et al. 2003b). In particular, the model succeeds in reproducing the basin wide structures of currents and sea level and temperature, and accurately simulates the Kelvin waves (Lengaigne et al. 2002), of particular importance for the current study. This model is also widely used in coupled mode for process studies (Guilyardi et al. 2001, 2003; Inness et al. 2003), paleoclimate simulations (Braconnot et al. 1999) and climate change experiments (Friedlingstein et al. 2001).

The atmospheric component of HadOPA is the atmospheric version of the met office unified model (UM), HadAM3. The model has a horizontal resolution of  $3.75^\circ$  longitude  $\times$   $2.5^\circ$  latitude, with 19 levels in the vertical, corresponding to a layer thickness of about 100 hPa in the mid-troposphere, but with higher resolution in the boundary layer and around the tropopause. Convection is parameterized using the mass-flux scheme of Gregory and Rowntree (1990), with the addition of convective momentum transport (Gregory et al. 1997). A more detailed description of this model and its performance in atmospheric model intercomparison project (AMIP)-type integrations can be found in Pope et al. (2000) and references therein. The quality of the AGCM simulation of ENSO has been studied extensively by Spencer and Slingo (2003) who showed that in the tropics, the UM displays considerable skill in capturing the associated precipitation and large scale circulation anomalies. In addition, Inness et al. (2001) have already performed a detailed analysis of the ability of HadAM3 to simulate aspects of tropical intraseasonal activity, associated, in particular, with the Madden Julian oscillation.

The atmospheric and oceanic components have been coupled through OASIS 2.4 (Valke et al. 2000) using a

coupling strategy similar to that of Guilyardi et al. (2001). No flux correction is applied. Air-sea fluxes and SST are exchanged every day.

## 2.2 Coupled model validation in the tropical Pacific

In this study, a 100-year control integration of HadOPA has been performed. The absence of any rapid (1–5 years) drift for most of the air-sea interface is notable, and the model is balanced—the radiative budget at the top of the atmosphere is close to zero and stays so for the 100 years. In the following, the model results have been evaluated against a range of observational data. These include weekly surface wind stress data derived from ERS-1 and ERS-2 scatterometers (Bentamy et al. 1996), weekly sea surface temperature (SST) data from Reynolds and Smith (1994), pentad precipitation data (CMAP; Xie and Arkin 1997), pentad mean outgoing longwave radiation (OLR) data from the National Oceanic and Atmospheric Administration (NOAA) polar orbiting satellites (Liebmann and Smith 1996) and daily acoustic Doppler current profile measurements from the tropical atmosphere ocean (TAO) moored buoy array (McPhaden et al. 1998). OLR from the model and observations have been used as a proxy for deep tropical convection. For compatibility with the other observational datasets, the OLR and TAO data were interpolated to weekly values.

## 2.3 Modeled climatology

Figure 1 displays the annual mean SST from the CGCM compared to the Reynolds and Smith (1994) climatological SST for the tropical Pacific. In general, the major features of the observed mean SST are simulated. No significant cold bias is observed in the western-central Pacific. However, the usual systematic warm bias in the sub-tropical eastern ocean basin is present (Fig. 1c)). Similarly, the South Pacific convergence zone (SPCZ) extends too far to the east and has too zonal an orientation, giving rise to the so-called double Inter-tropical convergence zone (ITCZ).

The tropical precipitation distribution in HadOPA captures many features of the observed climatology of Xie and Arkin (1997, Fig. 2a), but is affected by the model's SST errors. The unrealistic eastward extension of the southern Hemisphere warm-pool leads to a precipitation pattern that extends too far east over the SPCZ whilst the equatorial western Pacific displays a lack of precipitation (Fig. 2b). The simulated zonal wind stress is in relatively good agreement with the observations (Fig. 2c, d), although north of the equator (around  $10^\circ\text{N}$ ) the model overestimates the maximum values in the easterly trades by about 10%. Moreover, south of the equator, the weak trade winds, associated with SPCZ, extend too far in the central Pacific. Along the equator, the model's zonal wind stress is slightly weaker

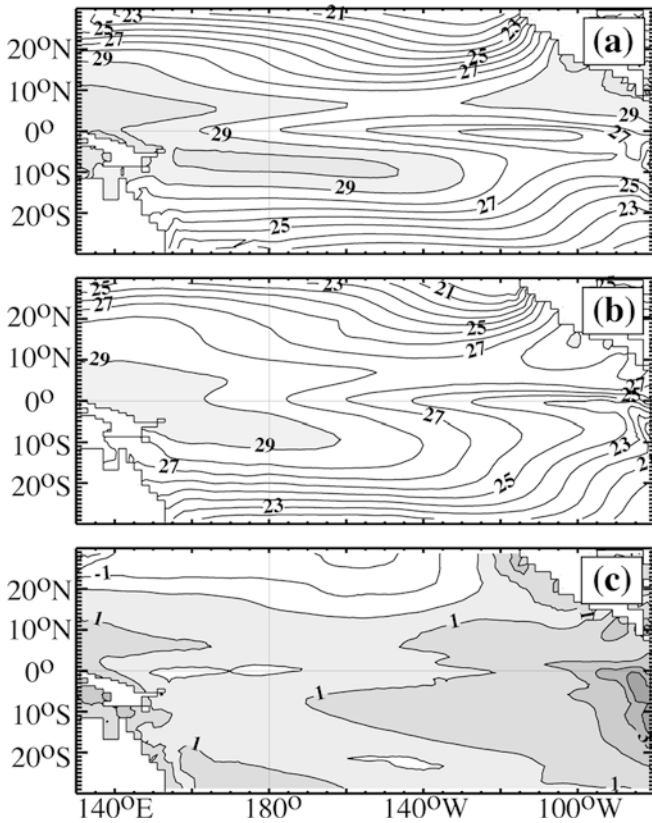
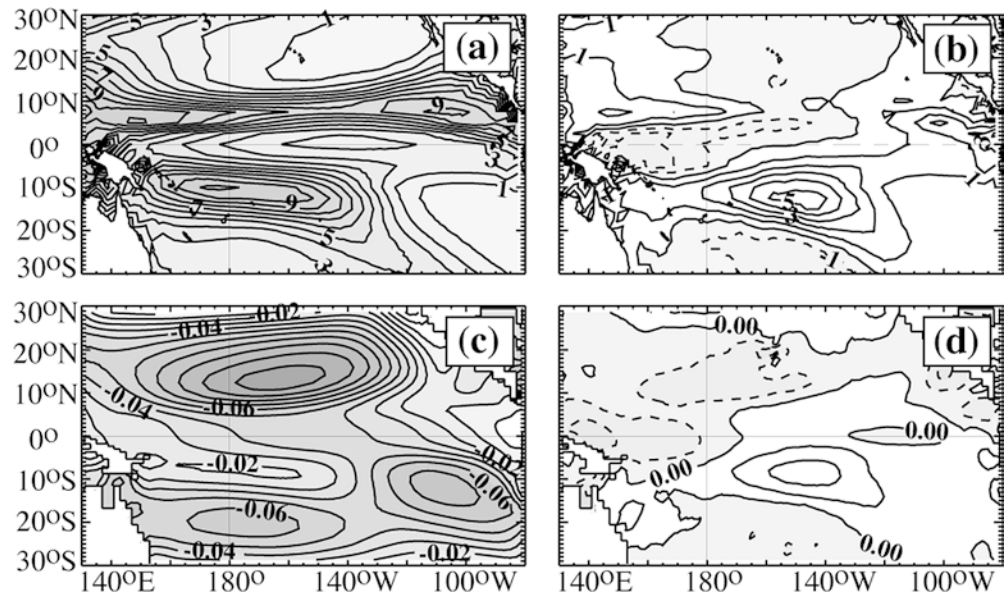


**Fig. 1** Annual mean field of the tropical Pacific SST of: the HadOPA coupled GCM (a), the Reynolds and Smith (1994)'s observations (b), and their difference (c). The contour interval is 1°C. Temperatures warmer than 29°C are shaded in (a), and (b). Positive contours are shaded in (c)

than observed in the central Pacific, but has an important negative bias over the western warm-pool. This equatorial behaviour is consistent with the underlying weaker SST gradient, with surface winds directed to-

**Fig. 2** Annual mean fields of tropical Pacific. **a** HadOPA precipitations. **b** HadOPA-CMAP precipitations. **c** HadOPA zonal wind stress. **d** HadOPA-ERS zonal wind stress. Contour intervals are  $1 \text{ kg m}^{-2} \text{ s}^{-1}$  for precipitations and  $0.01 \text{ N m}^{-2}$  for zonal wind stress. Negative contours are shaded and dashed in (b), and (d)



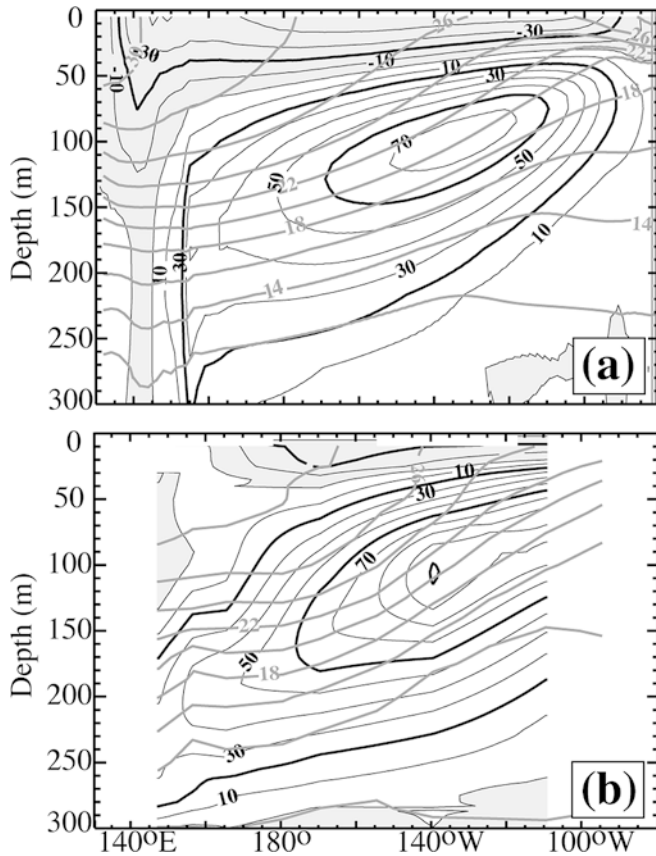
ward the warm SSTs south of the equator related to the double ITCZ.

The equatorial thermocline slope and structure, of importance for ENSO dynamics, are well reproduced by the coupled model (Fig. 3). The warm pool extends east of the dateline in agreement with observations but, as in forced mode (Lengaigne et al. 2003b), the thermocline is too diffuse. The zonal current structure is also reasonably well captured, although the intensity of the equatorial under current is underestimated by  $20 \text{ cm s}^{-1}$  and the SEC is too intense as compared to TAO array data. Both features are presumably due to a slightly weaker than observed equatorial trade winds in the central Pacific as the EUC intensity is mainly driven by the trade winds intensity through the zonal pressure gradient. Less eastward zonal momentum is therefore brought to the surface.

The simulation of the mean annual cycle of equatorial SST and zonal wind stress is compared with the observations in Fig. 4. The CGCM has a mean warm bias of approximately 2°C in the eastern Pacific. The zonal gradient of SST from the CGCM is realistically simulated in the central Pacific despite its reduced amplitude. The seasonal warming in early spring is also very well captured. The zonal wind stress seasonal cycle is remarkably reproduced by the CGCM, with two maxima in July and January in the central Pacific. The main model error occurs in the western Pacific, where the trade winds extend too far to the west, compared to the observations where they display nearly zero winds west of 160°E.

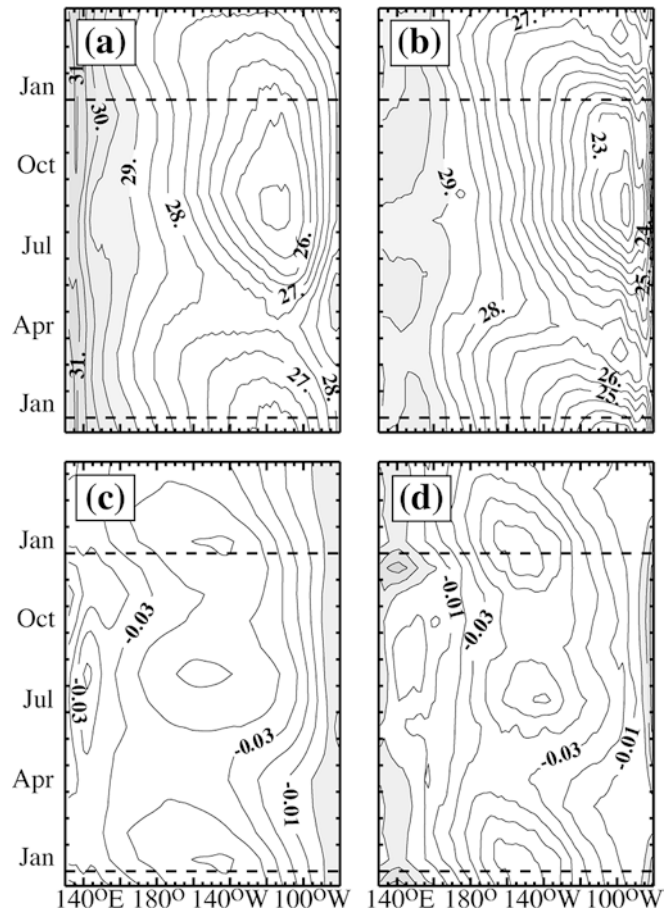
#### 2.4 Modeled interannual variability

Figure 5 illustrates the Niño 3 (150°W–90°W; 5°N–5°S) SST as well as the equatorial Pacific heat content anomalies over years 45 to 75 of the coupled simulation.



**Fig. 3** Equatorial section of mean zonal current (black lines) superimposed on temperature (grey lines) for the HadOPA model (a), and TAO moorings (b). Contour interval is  $10 \text{ cm s}^{-1}$  for the zonal current and  $2^\circ\text{C}$  for the temperature. Westward currents are shaded

As in the observations (Meinen and McPhaden 2000), the heat content anomalies generally lead changes in the anomalous SST. Strong interannual variability is evident, with El Niño event reaching a maximum amplitude around  $4^\circ\text{C}$ . However, periods of weaker interannual activity are found to occur, as is the case for years 58 to 65. We then compute standard deviations of monthly SST anomalies in the Niño 3, Niño 3.4 and Niño 4 regions as a simple measure of ENSO amplitude and structure in the simulation and observations (Table 1). The HadOPA model is producing a stronger variability than observations over the period 1950–2000. Standard deviations of monthly SST anomalies also suggest minimum variance over the western Pacific, with maximum in the eastern portion of the basin as is observed. Moreover, the model is able to simulate the seasonal phase locking of the SST variability with greater monthly standard deviations in boreal winter and decreased standard deviations in boreal spring (not shown). The simulated normalized power spectra of the Niño 3 monthly SST anomaly displays a first maximum power around 3.5 year as in the observations although the model's El Niño is much more regular than observed (not shown; see Guilyardi et al. 2004).



**Fig. 4** Time-longitude evolution of the seasonal cycle averaged over  $2^\circ\text{N}$ – $2^\circ\text{S}$  for HadOPA SST (a), Reynolds SST (b), HadOPA zonal wind stress (c), and ERS zonal wind stress (d). Contour are  $0.5^\circ\text{C}$  for SST and  $0.01 \text{ N m}^{-2}$  for zonal wind stress. Temperatures warmer than  $29^\circ\text{C}$  are shaded in (a), and (b). Positive contour are shaded in (c), and (d)

As will be shown in the next sections, an interesting feature of this coupled model for our study is the occurrence of spontaneous westerly wind events over the western Pacific. Their characteristics are in qualitative agreement with the time-space structure of observed westerly wind stress episodes over the western Pacific. However, the intensity of the simulated WWEs is generally underestimated, due mainly to the absence of the very strong WWEs, observed in nature (e. g. during the 1997–1998 El Niño).

### 3 Experiments design and ensemble results

#### 3.1 Experiments design

In two previous studies (Lengaigne et al. 2002, 2003a), by using both forced oceanic (OPA) and atmospheric (HadAM3) GCMs, the respective response of the ocean and the atmosphere to a strong WWE, that occurred during the 1997/1998 El Niño onset, was investigated. To study the full ocean-atmosphere coupled response to

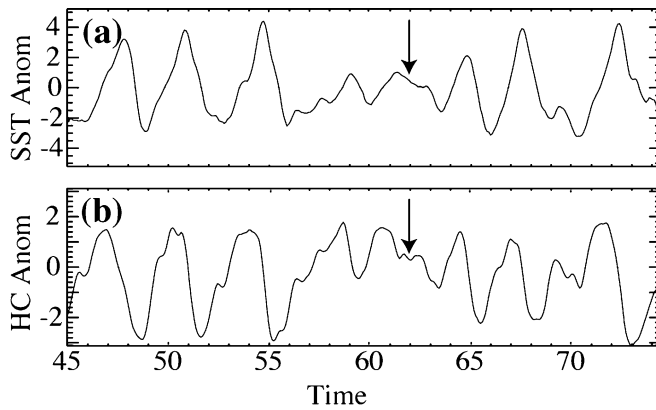


**Fig. 5** Time series of interannual anomalies for (a) the Niño 3 SST ( $^{\circ}\text{C}$ ) and (b) the equatorial Pacific ( $140^{\circ}\text{E}$ – $80^{\circ}\text{W}$ ;  $5^{\circ}\text{N}$ – $5^{\circ}\text{S}$ ) heat content ( $10^{22}$  J) in the upper 300 m for HadOPA from year 1945 to 1975. The anomalies are smoothed with a 5-months running mean. The arrow indicates the initial state of CREF and CWWE ensembles

a WWE, two ten member ensemble integrations, starting from slightly perturbed initial conditions, have been conducted with the HadOPA CGCM. To perturb atmospheric initial conditions, ten successive model days were taken for the atmospheric initial states of the ensemble, whilst the ocean initial condition remained unchanged. All the experiments were started on 1 December 1961 and ended in May 1963. This period was selected since it is characterised by a relatively low ENSO activity as shown in Fig. 5a. Moreover, the initial state of the coupled experiments in December 1961 is characterised by a slightly positive ocean heat content along the equator in late 1961 (Fig. 5b), favourable to the development of a warm event (Meinen and McPhaden 2000). Note that the response of the coupled system to a WWE with a significant heat deficit along the equator in the ocean initial conditions is likely to be very different.

The purpose of the present study is to test if a strong WWE is able to trigger El Niño events from the previous ocean-atmosphere conditions. In the reference ensemble (CREF ensemble), the members run freely without any wind stress perturbation whereas, in the perturbed ensemble (CWWE ensemble), a strong WWE is added by applying a zonal wind stress anomaly at the ocean-atmosphere interface in the western Pacific in February 1962 (no meridional wind stress anomaly is applied). The applied westerly wind stress anomaly in each

**Table 1** The Standard deviations SD ( $^{\circ}\text{C}$ ) of Niño 3, Niño 3.4 and Niño 4 monthly time series in the simulation and the observations. The SD are computed during the 1950–2000 period for the observations and during the 100 years of the integration for the model experiment

	Niño 4	Niño 3.4	Niño 3
HadOPA	1.37	1.68	1.78
Observations	0.63	0.88	0.93

member of CWWE ensemble captures the positive zonal wind stress anomaly associated with the WWE observed in early 1997, which is described in Lengaigne et al. (2002). This intense WWE reaching  $0.15 \text{ N m}^{-2}$  at the equator lasted about a month and extended zonally over more than  $30^{\circ}$ , from  $135^{\circ}\text{E}$  to  $170^{\circ}\text{E}$ , and meridionally from  $5^{\circ}\text{N}$  to about  $15^{\circ}\text{S}$ . This event can be considered as an S-type event in the classification of Harrison and Vecchi (1997). The wind stress perturbation is introduced in the coupled system on 20 January and ended in late February. This recognises that the boreal winter is a period where strong WWE activity preferentially occurs in the observations. Moreover, at that time, the modelled warm-pool and convective activity both extend to the dateline (Fig. 6a), which is physically consistent with the occurrence of a strong WWE extending to  $170^{\circ}\text{E}$ .

In this study, we restricted our analysis from February 1962 through to May 1963 for two reasons. First, initializing the CGCM one month and a half prior to this period allows the internal atmospheric variability between each member in the ensemble to be decorrelated. However, because the ocean is the slowly varying component of the coupled system, the ocean mean states of each individual run in the ensemble experiment remain strongly correlated. Secondly, since the upper limit of ENSO predictability appears to be limited to be about 12 months (see Collins 2002), we therefore restrict our analysis to 1 year following the introduction of the WWE.

### 3.2 Ensemble results

Figure 6 displays the SST response along the equator for CREF and CWWE mean ensemble averages as well as their differences. The initial state of the equatorial SST in CREF ensemble is slightly warmer than the mean modelled climatology but the SST of the reference ensemble evolves toward its climatological value at the end 1962 (Figs. 4a and 6a). The insertion of a WWE at the beginning of the year strongly modifies the evolution of the ensemble mean. The mean response of the coupled model to the insertion of a WWE consists of an El Niño-like warming of the central eastern Pacific (up to  $2^{\circ}\text{C}$ ) that reaches its maximum intensity roughly 9 months after the event (in November–December 1962; Fig. 6c). Moreover, this insertion shifts the warm pool eastward by about  $20^{\circ}$  and the upwelling in the eastern Pacific is significantly reduced for the whole year. However, this averaged view does not illustrate the large diversity of behaviour between the ensemble members. To that end, the Niño 3 anomaly according to the mean SST of CREF ensemble is shown in Fig. 7 for each individual member of both ensembles. In this study, the departure from the reference mean state (neutral, moderate and strong warming, moderate and strong cooling) is defined as follows. Every individual member of an ensemble whose mean SST anomaly remains within  $\pm 0.6^{\circ}\text{C}$  of the CREF ensemble mean over the 6 months following the

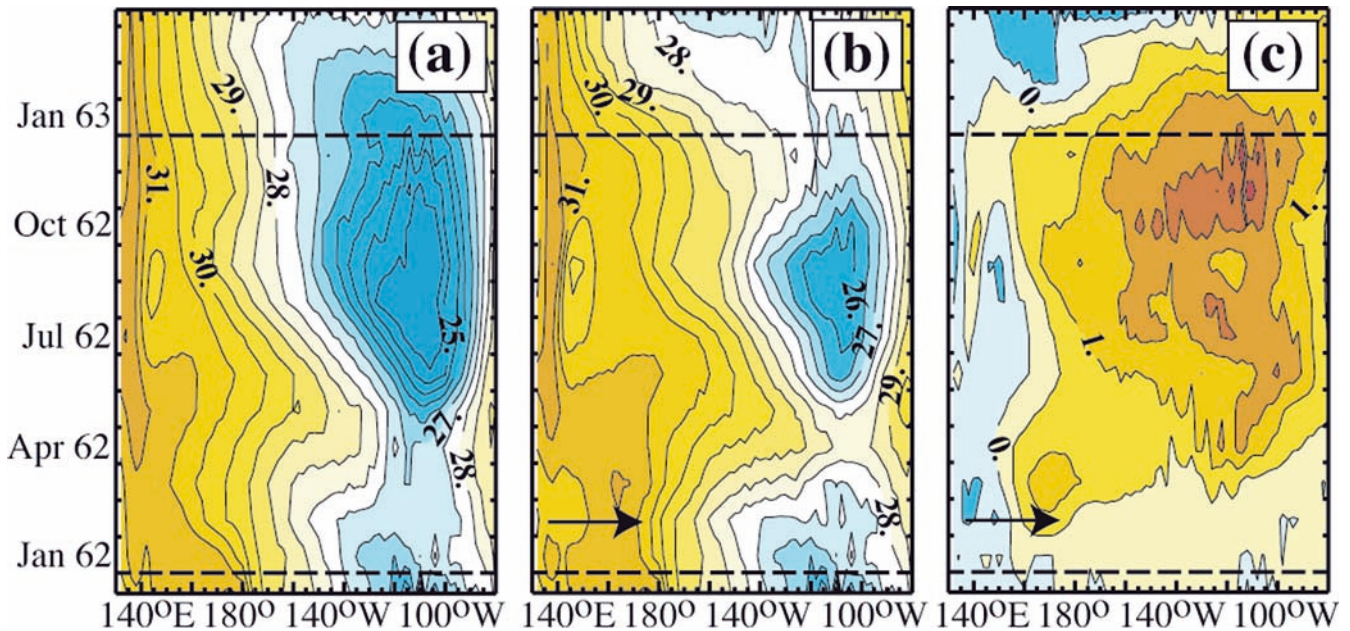


**Fig. 6** Time longitude evolution of SST averaged over  $2^{\circ}\text{N}$ – $2^{\circ}\text{S}$  for CREF ensemble mean (a), CWWE ensemble mean (b), and their difference (c). The contour interval is  $0.5^{\circ}\text{C}$  for temperature. The arrow denotes the artificially introduced WWE

inserted WWE (from March to August) will be considered as a neutral case (black thin lines in Fig. 7). Individual members whose mean SST anomaly remains between  $+0.6$  and  $+1.2^{\circ}\text{C}$  (respectively  $-0.6$  and  $-1.2^{\circ}\text{C}$ ) will be considered as a moderate warming (green lines) (respectively moderate cooling (blue line)) compared to the mean reference SST evolution. Finally, members whose mean SST anomaly exceed  $+1.2^{\circ}\text{C}$  will be considered as a strong warming (red lines). There are no correspondingly strong cooling events.

Figure 7a shows that relatively small perturbations to the atmospheric initial conditions can lead to a quite rapid divergence of the ensemble members, i.e. the system does appear to exhibit sensitive dependence on initial conditions, indicating a loss of predictability within one year, consistent with Collins (2002). However, in the first two months of the experiment, the oceanic state of each individual members remains strongly correlated when the WWE is added to the coupled system (arrow in Fig. 7b). In the control (CREF) ensemble, one experiment can be considered as a moderate warming (green curve), seven as neutral cases (black curves), one as a moderate cooling (blue curve) and one as a strong warming (red curve). This last CREF ensemble member corresponds to a strong El Niño event, associated with the occurrence of a series of WWEs from March to May over the western warm-pool (not shown). These WWEs, naturally generated by the coupled model physics, are likely to trigger the simulated El Niño event in this CREF ensemble member.

In the CWWE ensemble (Fig. 7b), the insertion of a WWE in February 1962 strongly influences the evolution of the ensemble members. Out of ten members, four

developed in a strong warming (red curves Fig. 7b), four are characterized by a moderate warming (green curves) and two remain in neutral conditions (black curves). No

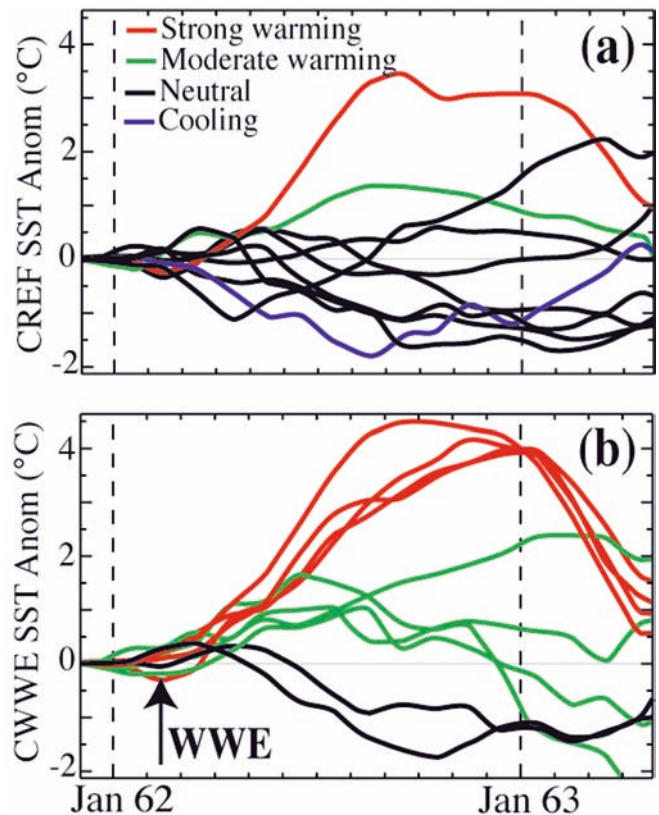


**Fig. 7** Time series of Niño 3 SST anomalies compared to CREF ensemble mean for CREF ensemble members (a), and CWWE ensemble members (b). The red lines correspond to strong warming cases, the green ones to moderate warming cases, the black ones to neutral cases and the blue one to a moderate cooling case. The arrow denotes the artificially introduced WWE

cold events are produced. The monthly SST anomalies of CREF and CWWE ensemble are statistically different at 95% significance level for the 9 months following the WWE introduction in CWWE ensemble (see Appendix). These results indicate that intense WWEs act to modify significantly the coupled ocean-atmosphere system. However, there is a marked diversity in the coupled system response to WWEs. Even though some members developed into strong El Niños (red curves in Fig. 7b), a few others do not seem to be significantly influenced by the WWE introduction (black curves in Fig. 7b). To fully assess the role of WWEs, it is therefore essential to understand the different mechanisms that lead to the diversity in the CWWE ensemble members evolution.

To that end, the time-evolution of the eastern edge of the warm-pool (hereafter “EEWP”; defined as the  $30^{\circ}\text{C}$  isotherm in the coupled model) and the extent of the easterly trade winds are shown in Fig. 8 for each member of the CWWE ensemble (thin solid lines) and for the mean CREF ensemble average (thick dashed line). The evolution of the EEWP is fundamental since it is associated with the eastward extension of the convective and

WWE activity over the tropical Pacific and has therefore strong implications for ENSO (Picaut et al. 1996). In the 3 months following the event, the EEWP in all the CWWE members remains further east than in its mean evolution in the CREF ensemble (Fig. 8a). However, the evolution of the EEWP differs strongly between each ensemble member. In the four strong warming cases (red curves in Fig. 8a) the EEWP is shifted eastward by about  $30^{\circ}$  longitude during the 3 months following the WWE. In contrast, it is only displaced by  $10$  to  $15^{\circ}$  in the first few months following the WWE and then goes back close to mean CREF evolution in the two neutral cases (black curves in Fig. 8a). This zonal displacement of the warm pool coincides with a reduction of the zonal extension in the trade winds (Fig. 8b), defined as the  $-0.01 \text{ N m}^{-2}$  zonal wind stress isoline. The more the EEWP is displaced eastwards, the stronger are the westerly (positive) zonal wind stress anomalies in the western-central Pacific and the more the trade winds are confined in the eastern part of the basin. In the following section, we will focus on one individual member of each typical case (neutral, weak and strong warm cases) to describe in more details the mechanisms by which their trajectories diverge.

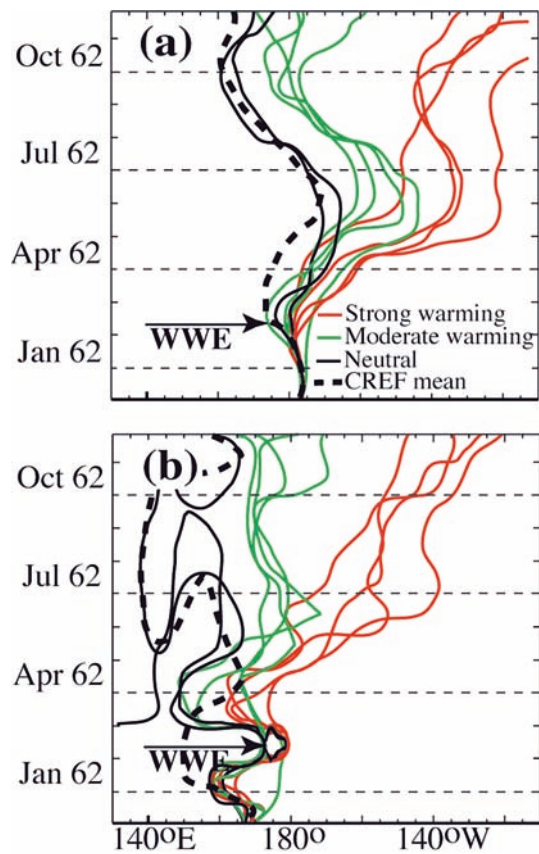


**Fig. 8** Time longitude evolution for CWWE ensemble members (thin solid lines) and CREF ensemble mean (thick dashed line) averaged between  $2^{\circ}\text{N}$  and  $2^{\circ}\text{S}$  for the eastern edge of the warm-pool ( $30^{\circ}\text{C}$  isotherm) (a), and the  $-0.01 \text{ N m}^{-2}$  isoline (b). The red lines correspond to the strong warming cases, the green ones to moderate warming cases and the black one to neutral cases. The arrow denotes the artificially introduced WWE

#### 4 Evolution of three representative individual members of CWWE ensemble

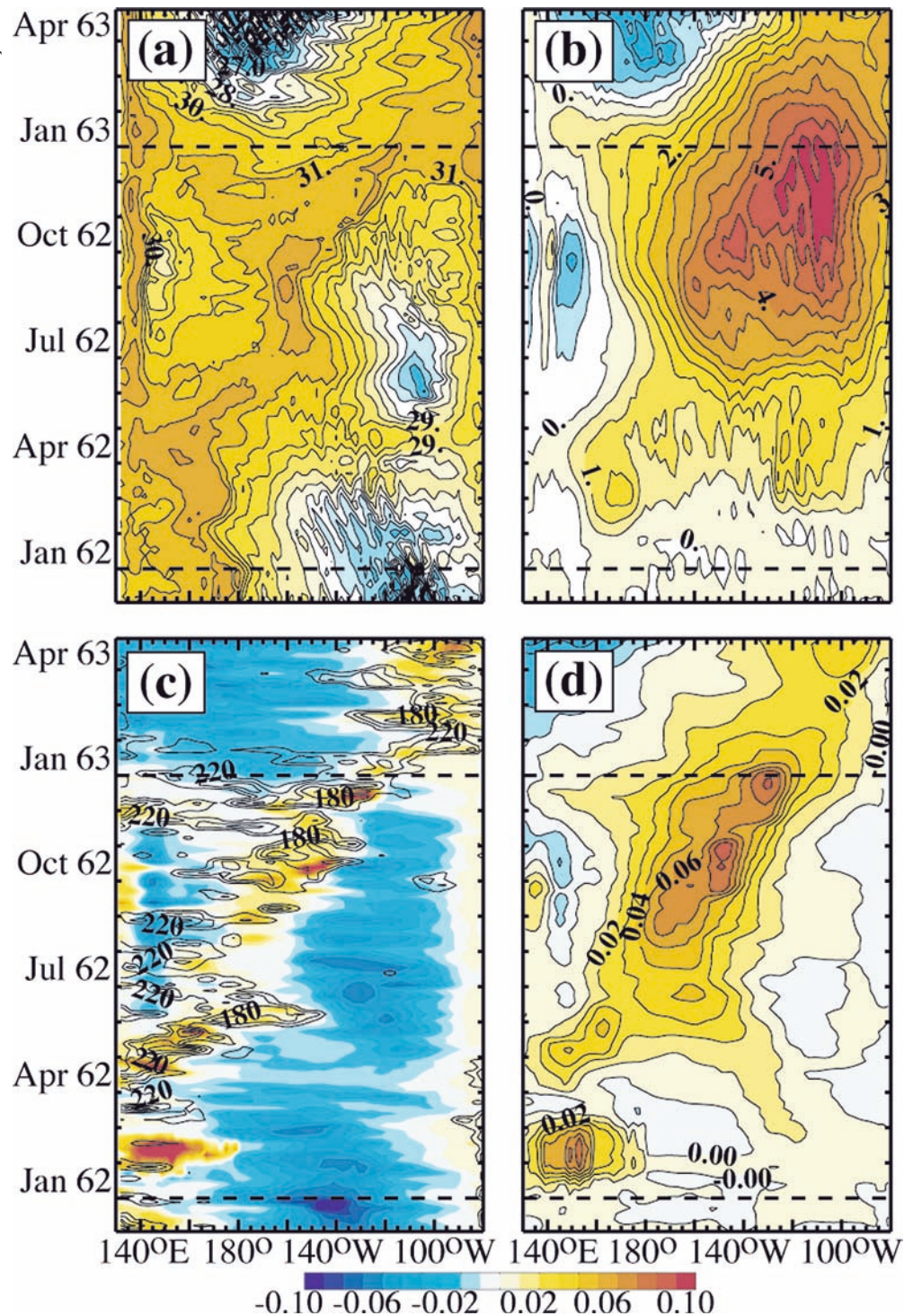
##### 4.1 The strong warm cases

In this part, one of the strong warm cases (red curves in Figs. 7 and 8) has been selected (named hereafter SW experiment) to illustrate the mechanisms that lead to the development of a strong El Niño event when an intense WWE is inserted. All the mechanisms discussed for this particular experiment are qualitatively representative of the other strong El Niño cases (i.e. the three other red curves of CWWE and the one that naturally occurs in the CREF ensemble in association with a strong WWE activity in spring 1962 (red line in Fig. 7a)).

Figure 9 displays the time-evolution of the SST and zonal wind stress along the equator for SW experiment, and the corresponding differences with respect to the CREF ensemble mean. In agreement with the former forced OGCM study (Lengaigne et al. 2002), the ocean response to a strong WWE is characterized by three specific SST responses in the 2 months following the event (Fig. 9b): a weak local cooling over the far-western Pacific (west of  $150^{\circ}\text{E}$ ) and two warmings, one remote in the central/eastern Pacific (east of  $160^{\circ}\text{W}$ ) and one around the dateline. The weak cooling is a common feature of all the experiments. It is mainly associated with the vertical advection of cold waters from the thermocline to the upper layers. As the heat fluxes are not explicitly modified in the SW experiment (no heat flux anomaly is applied), this weak local response, when compared to observations (Vecchi and Harrison 2000), is consistent with the results of Cronin and McPhaden



**Fig. 9** Time-longitude evolution for SW experiment averaged between 2°N and 2°S for the SST (a), the SST anomaly compared to CREF ensemble mean (b), the zonal wind stress superimposed on OLR lower than  $220 \text{ W m}^{-2}$  (c), and the zonal wind stress anomaly compared to CREF ensemble mean (d). The anomalies are smoothed to remove sub-monthly variability. The contour interval is  $0.5^\circ\text{C}$  for temperature,  $0.01 \text{ N m}^{-2}$  for zonal wind stress and  $20 \text{ W m}^{-2}$  for OLR

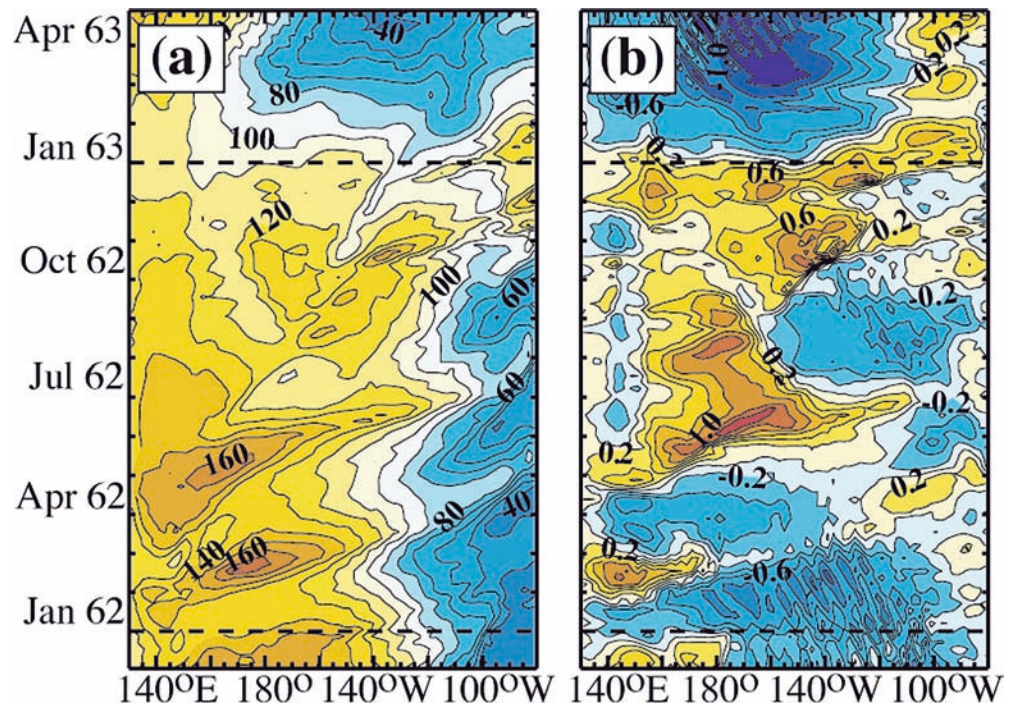


(1997) who argue that this local cooling is mainly driven by heat flux perturbations (increased latent heat flux and decreased shortwave radiation) associated with a WWE.

The second response consists of a strong warming in the central/eastern Pacific from March onwards. This warming is associated with the generation of a strong downwelling Kelvin wave by the inserted WWE. This wave propagates eastwards from the WWE region to the eastern Pacific, depressing the equatorial thermocline by

about 40 m until it reaches the eastern boundary in mid-May (Fig. 10a). This wave initiates a central/eastern Pacific warming that exceeds  $2^\circ\text{C}$  at  $120^\circ\text{W}$  in April, 2 months after the WWE occurrence (Fig. 9b). This warming is a common feature associated with the Kelvin wave generation in both modelling (Giese and Harrison 1991; Lengaigne et al. 2002) and observational studies (Vecchi and Harrison 2000; McPhaden 2002). However, its amplitude, relatively large in this case, exceeds that

**Fig. 10** Time longitude evolution for SW experiment averaged between 2°N and 2°S for depth of the 20°C isotherm (a), surface zonal currents (b). The contour interval is 10 m for the 20°C isotherm depth and 0.2 m s<sup>-1</sup> for currents



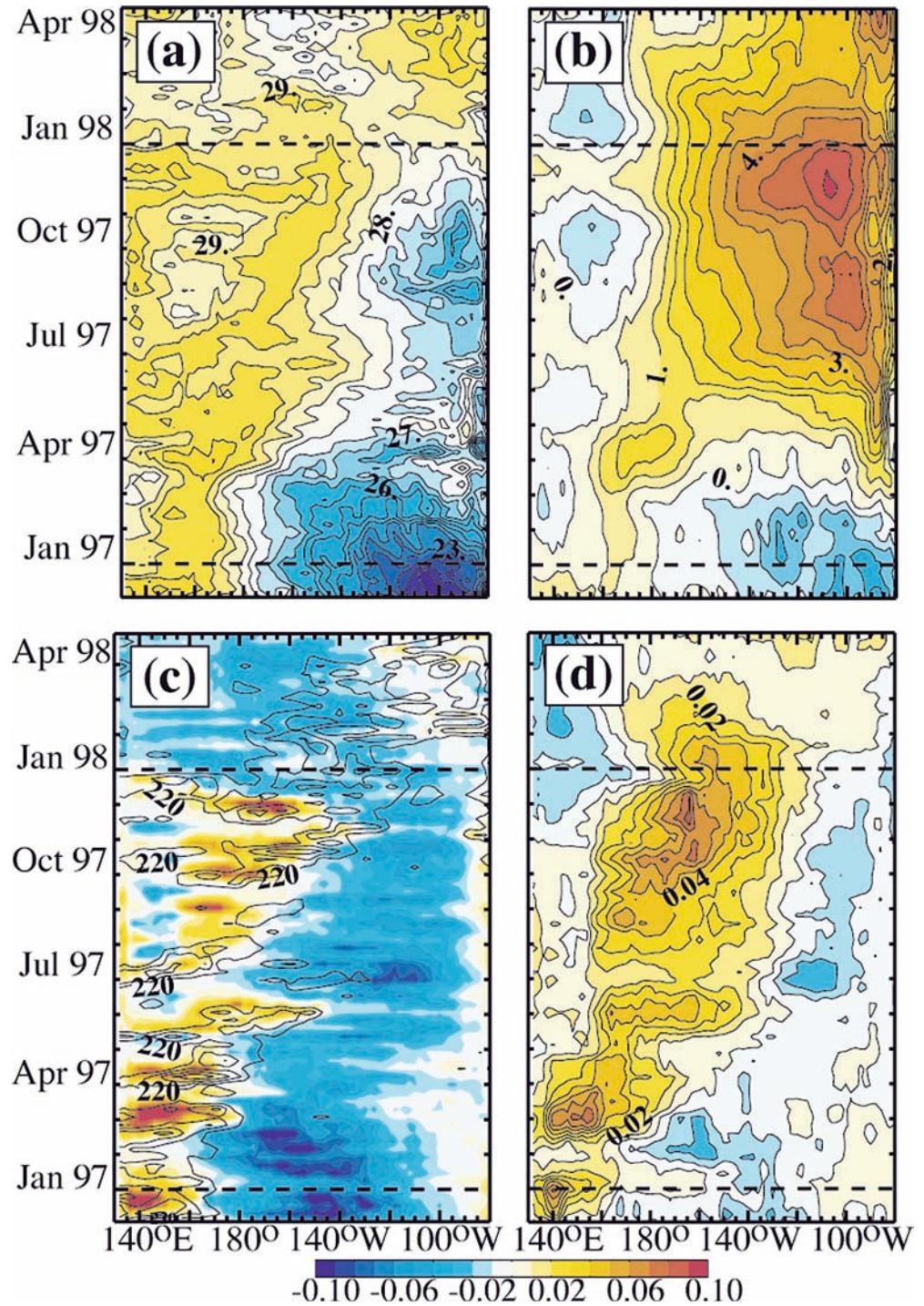
derived from the previous oceanic forced modelling studies. This point will be discussed further in Sect. 6.

The third SST response occurs over the western Pacific warm-pool in the months following the inserted WWE (Fig. 9b). It consists of the strong SST anomaly (up to 1.5°C) near the dateline, displacing eastward from March to May, and illustrative of an eastward displacement of the warm-pool by 30° longitude in the 2 months following the event (Fig. 9a). This displacement is triggered by the zonal current anomaly associated with the wind-forced Kelvin wave (Fig. 10b) and promotes the occurrence of subsequent WWEs from April to early June (Fig. 9c), naturally generated by the atmosphere model physics (Lengaigne et al. 2003a). These subsequent WWEs favour an El Niño development in two ways. First, they warm the central-eastern equatorial Pacific through the generation of further downwelling equatorial Kelvin waves. The series of WWEs that occurs from the end of April to the end of May again depresses the thermocline by 40 m in July (Fig. 10a), advects warm waters eastward, reduces the equatorial upwelling, and therefore acts to prolong warm conditions in the central-eastern Pacific. Second, these WWEs are responsible for the generation of intense eastward currents (Fig. 10b; up to 1.4 m s<sup>-1</sup> in mid-June) that rapidly advect eastwards the EEWP from the dateline in early May to 140°W at the end of June (Fig. 9a). This further enhances the eastward shift of convective activity (Fig. 9c) and the concurrent development of westerly wind anomalies in the central Pacific (Fig. 9d). Then, from June to August, the WWE activity is strongly reduced over the western and central Pacific warm waters (Fig. 9c). This reduced activity and the concomitant seasonal reinforcement of the trade winds

in the eastern Pacific stops the eastward progression of warm waters, maintaining the EEWP at about 140°W from June to September (Fig. 9a). The renewal of the WWE activity in phase with the seasonal cycle (from October to December) once again shifts warm waters eastwards, which reach the eastern boundary in the early part of year 63. This results in a maximum SST anomaly of about 5.5°C at 110°W in December. From then on, the western/central Pacific cools, and switches to a cold state. The rapid and successive eastward shifts of the warm pool associated with intense WWE activity in spring and autumn are essential features that explain the development phase and the intensity of this El Niño event. The mechanisms associated with this warm water displacement, through the generation of the intense long-lasting eastward jets displayed in Fig. 10b, will be discussed further in Sect. 6.

To evaluate the model results, observed SST, zonal wind stress and their corresponding anomalies are presented in Fig. 11 for the 1997/1998 El Niño. The modelled El Niño event compares qualitatively well with the observations. As in the SW experiment, the strong WWE observed from mid-February to mid-March is likely to be responsible for the initial warming of the central-eastern Pacific (up to 2°C at the end of May) and the SST anomaly around the dateline in early 1997 associated with the eastward displacement of the warm-pool (Fig. 11b). As in the SW experiment, this initial shift is followed by further convective and WWE activity from April to June (Fig. 11c), associated with an eastward extension of the warm-pool to 140°W in June. This displacement and subsequent WWE activity is associated with a rapid warming of the central eastern Pacific, reaching 4°C in July. From then on, the El Niño is fully

**Fig. 11** As Fig. 9 but for the 1997/1998 observations (Reynolds and Smith (1994)'s SST and ERS zonal wind stress). Anomalies are relative to the mean seasonal cycle

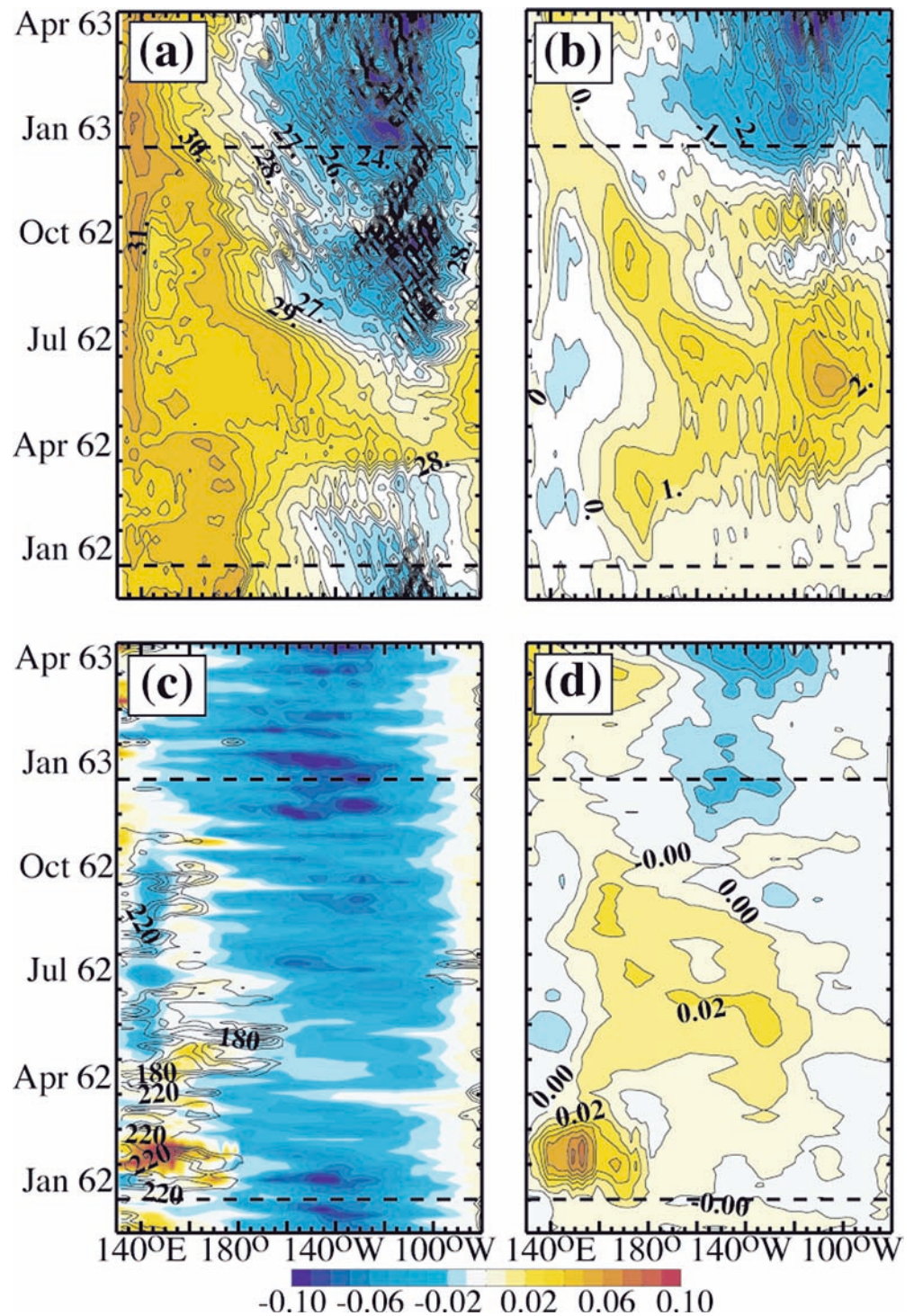


developed and the warm-pool extends further east in association with a strong WWE activity in late 1997. The convective activity, accompanying the warm waters, reaches the eastern boundary in early 1998 whilst the western central Pacific starts to cool. All these features in the observations are well captured in the model simulation. The remaining differences between the model and observations are mostly due to the mean biases of the coupled model (i.e. a warm-pool and an eastern Pacific that are generally too warm).

#### 4.2 The moderate warm cases

In this part, one of the moderate warm cases (green curves in Figs. 7b and 8) has been selected (named hereafter MW experiment) to illustrate the main features associated to this type of event and the main mechanisms that actually prevent them from developing into strong El Niño events. All the features discussed in this section for this particular case are also representative of the other moderate warming cases of CWWE ensemble.

**Fig. 12** As Fig. 9 but for MW experiment



The initial coupled response to a WWE in this case is close to the one found in the strong warm cases (Fig. 12). During the 2 months following the imposed WWE, the central-eastern Pacific is warmer by more than 2°C and a strong SST anomaly is generated at the EEWP, displaying an eastward displacement of warm waters (Fig. 12a, b). However, compared to the strong warming cases, only weak WWEs occur in the following months (Fig. 12c, d). In particular, when the trade winds

strengthen in June–July, in agreement with the seasonal cycle, only a weak WWE activity is observed over the western warm-pool. The moderate WWE that occurs in May does not significantly affect the central-eastern Pacific; no significant deepening of the equatorial thermocline is observed (Fig. 13a) in contrast to that in the SW experiment in July (Fig. 10a). Moreover, this event only generates a local intensification of the zonal current during the 2 weeks of the WWE, but is not strong en-

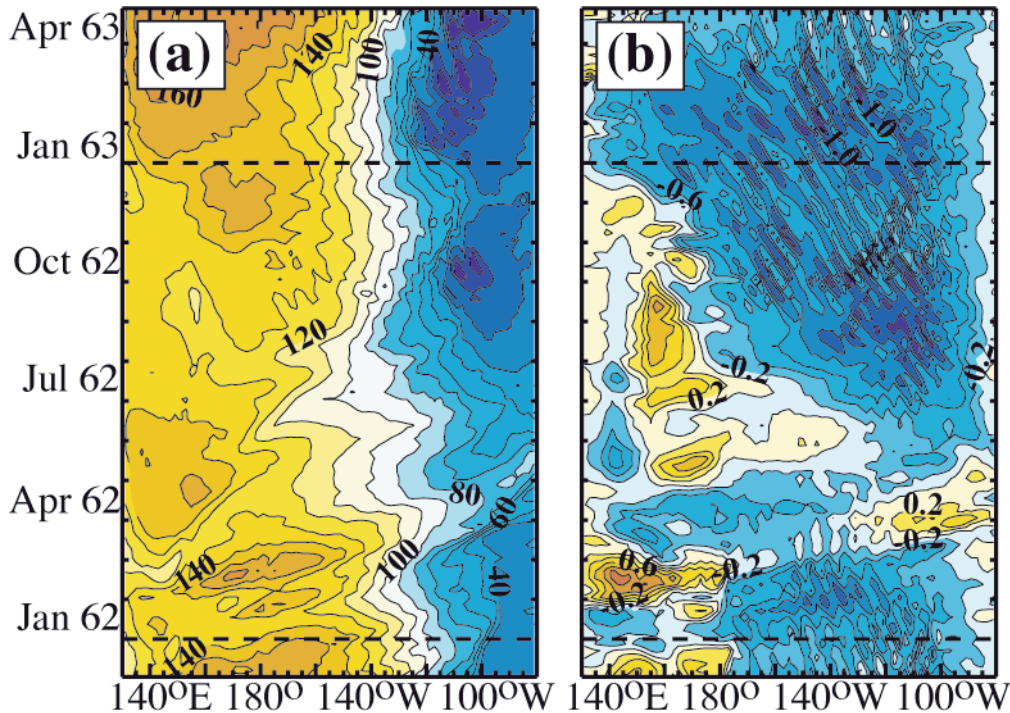


**Fig. 13** As Fig. 10 but for MW experiment

ough to initiate an eastward intensification of the currents at the EEWP (Fig. 13b). At this time, no surface jet is therefore able to counter the seasonal strengthening of the south equatorial current driven by the trade winds. From June to August, the warm-pool is shifted back to the western Pacific by  $30^\circ$  longitude (Fig. 12a). However, the warming in the central-eastern Pacific persists over most of the year, but decays from June to be negligible in December. The reduced eastward extension of the warm-pool in this case significantly weakens the zonal wind stress anomalies found in the western-central Pacific from June onwards, compared to the strong warming cases. This results in weaker SST anomalies in the central-eastern Pacific due to a reduced Kelvin wave forcing. Thus, this lack of positive feedback results in a moderate warming that tends to peak in June.

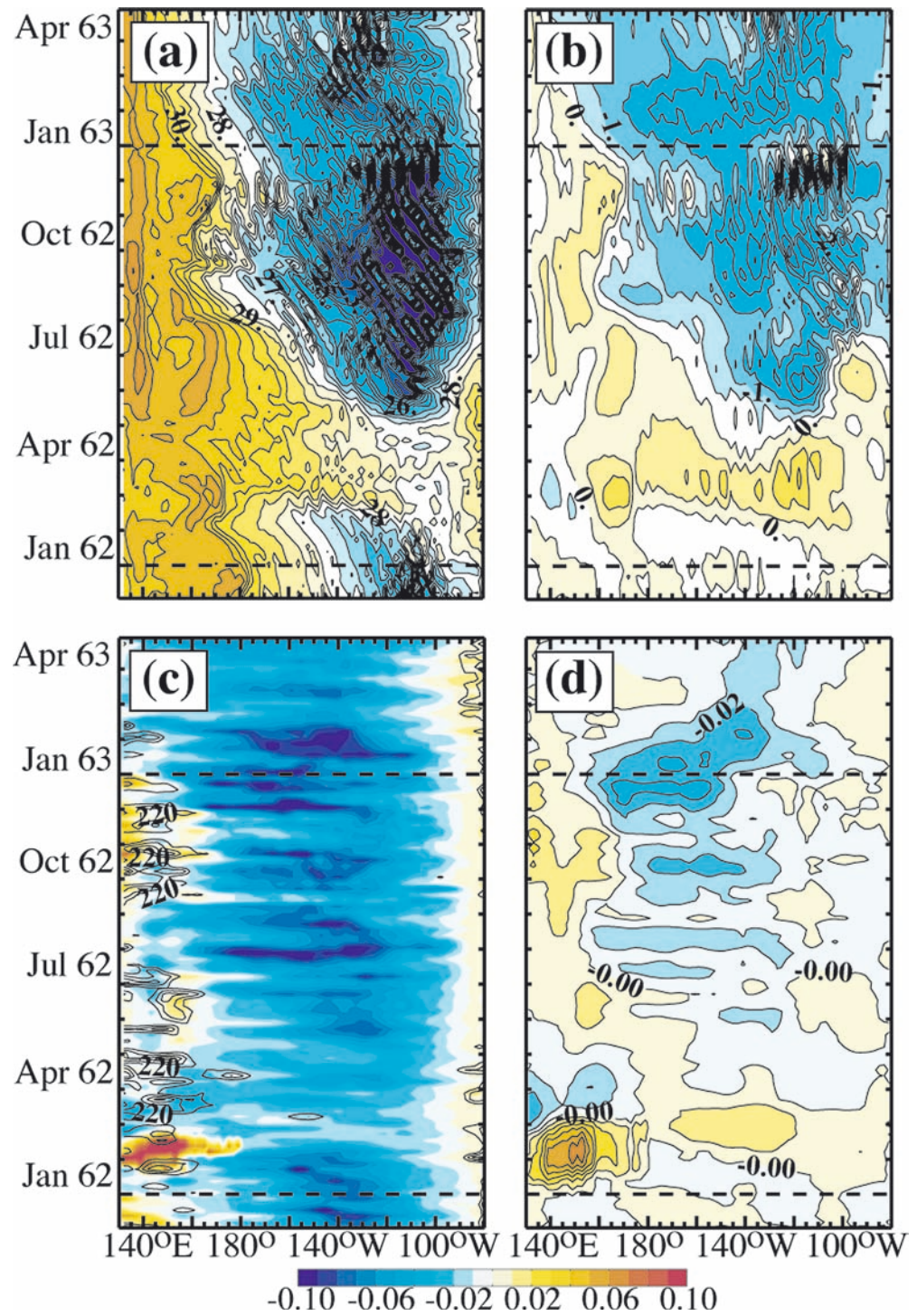
A weak WWE activity in spring and a westward shift of the warm-pool in July are features common to all moderate warming cases (Fig. 8a). Table 2 summarizes the mean WWE activity that occurs from March to June (i.e. after the artificially introduced WWE) for every type of response in the CWWE ensemble, following the classification of Lengaigne et al. (2003a). Any period of westerly winds (averaged between  $3^\circ\text{N}$ – $3^\circ\text{S}$ )

east of  $130^\circ\text{E}$  whose maximum zonal windstress,  $\tau_x$ , is greater than  $0.02 \text{ N m}^{-2}$  and lasts for more than 5 days is considered a WWE. Three types of WWEs are defined: type I ( $0.02 \text{ N m}^{-2} < \tau_x < 0.05 \text{ N m}^{-2}$ ), type II ( $0.05 \text{ N m}^{-2} < \tau_x < 0.08 \text{ N m}^{-2}$ ) and type III ( $\tau_x > 0.08 \text{ N m}^{-2}$ ). Based on this procedure, an average of 1.5 strong WWEs (type III) occur in the strong warm cases whereas no such events are found in the moderate warm case. These moderate warmings are instead characterized by the occurrence of weak WWEs (type I), resulting in a reduced oceanic impact as described above. However, in these four moderate cases, the insertion of a WWE at the beginning of the year systematically warms the Pacific and displaces the EEWP and the convective zone by  $20^\circ$  longitude until late 1962 (Fig. 8a). Similar results have been obtained by Latif et al. (1988) in a coupled ocean-atmosphere study. In their study, the insertion of a WWE at the beginning of the year modifies the mean conditions by shifting the warm-pool and the convective area by  $20^\circ$  longitude for most of the year. Nevertheless, their SST and zonal wind stress anomalies did not propagate and no warming occurred in the central-eastern Pacific. They associated this weak eastern Pacific response to their model biases (coarse atmospheric resolution, ocean model too inert, weak atmospheric response to SST anomalies) and to

**Table 2** Mean number of WWE for each type of CWWE ensemble members (strong warming, moderate warming, neutral). WWEs are divided in three types depending on their intensity (see text)

Mean number of WWE	Type of WWE		
	Type I ( $0.02 \text{ N/m}^2 < \tau_x < 0.05 \text{ N/m}^2$ )	Type II ( $0.05 \text{ N/m}^2 < \tau_x < 0.08 \text{ N/m}^2$ )	Type III ( $\tau_x > 0.08 \text{ N/m}^2$ )
Strong warming (4 members)	2.75	1.25	1.5
Moderate warming (4 members)	3.0	0.25	0.0
Neutral (2 members)	0.5	0.0	0.0

**Fig. 14** As Fig. 9 but for NC experiment



the flux correction method employed that acts to damp the SST anomalies.

#### 4.3 The neutral cases

Over ten ensemble members, only two of them remain in neutral (slightly cold) conditions. The SST, zonal wind stress and their corresponding anomalies are presented in Fig. 14 for one of these cases (named hereafter NC

experiment). Its evolution, even in its initial phase, strongly differs from the previous warming cases. The SST signal in the central eastern Pacific along the Kelvin wave path is strongly damped, reaching at best 0.5°C at 120°W. In the same way, the eastward shift of the warm-pool is less pronounced and does not persist for more than 2 months (Fig. 14a, b). This weak initial impact of the WWE on the equatorial Pacific prevents the development of strong positive coupled feedbacks and no subsequent WWE activity occurs over the warm-pool

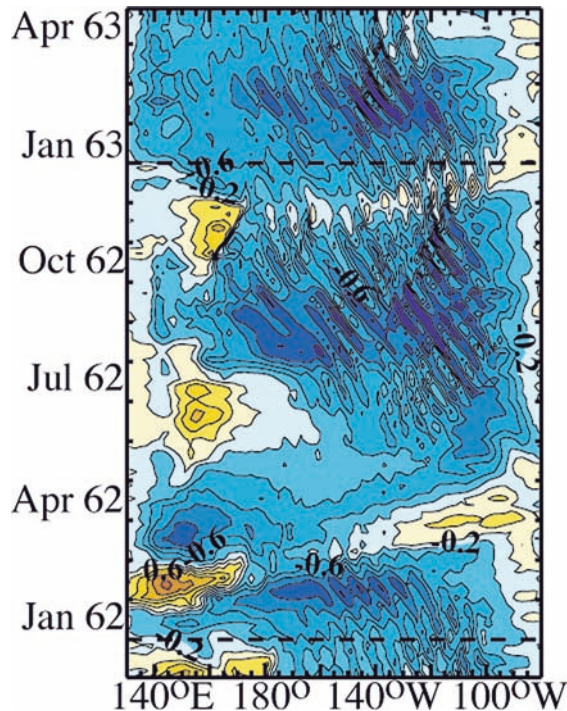


**Fig. 15** Time longitude evolution for NC experiment for surface zonal currents averaged between 2°N and 2°S. The contour interval is  $0.2 \text{ m s}^{-1}$

(Fig. 14c, d). The positive SST signals therefore disappear in the two months following the inserted wind event.

The reasons for such a limited impact of the WWE are associated with internal atmospheric variability during and following the inserted WWE. In fact, the ocean is the slowly varying component of the coupled system and, at the time of the WWE, its state mainly resembles the nine other members of the CWWE ensemble. More work is needed to identify precisely the reason for such a weak response, although it could be hypothesized that a strengthening of the trade winds over the equatorial Pacific due to internal atmospheric processes may be the main cause of this response. In fact, in March–April, following the inserted WWE, the trade winds strengthened over the western Pacific warm-pool (Fig. 14c, d), producing stronger westward zonal currents (up to  $-1.1 \text{ m s}^{-1}$ ) in March–April (Fig. 15) compared to SW and MW experiments (up to  $-1.1 \text{ m s}^{-1}$  compared to  $-0.6 \text{ m s}^{-1}$  in SW (Fig. 10b) and MW cases (Fig. 13b)). These currents act therefore to counter the impact of the WWE on the warm-pool and to shift immediately warm waters back to the western Pacific. In the same way, a reinforcement of the trade winds in the central eastern Pacific at the time of the WWE could result in the reduction in warming east of the dateline. This could act to damp the downwelling and advection of warm water associated with the remote Kelvin wave forcing and therefore limits the eastern and central Pacific warming. The reason for such a reinforcement of the trade winds in the coupled model re-

mains however to be understood. Episodic trade winds events are frequently observed over the warm-pool during the 1993–2001 period but their intensity rarely reaches that simulated by the coupled model in March 1962 of the NC experiment.

## 5 Coupled processes involved in El Niño onset

In this study, two coupled processes associated with the occurrence of WWEs have been identified in the onset and development of El Niño: (1) the warming of the central eastern Pacific generated along the Kelvin wave path, and (2) the eastward shift of the warm-pool associated with the occurrence of oceanic eastward surface jets. Each of these processes will be detailed in this section.

As shown in Figs. 9b and 12b, a warming of the central-eastern equatorial Pacific reaching a maximum amplitude ranging from  $1.5$  to  $2.5^\circ\text{C}$  60 days following the inserted WWE is characteristic of eight of the ten CWWE ensemble members (the strong and moderate warming cases). This warming associated with a WWE has already been noticed in previous forced OGCM studies (Giese and Harrison 1991; Lengaigne et al. 2002), but its intensity is considerably stronger. In fact, all these forced studies estimate the warming along the Kelvin wave path to be between  $0.5$  and  $1^\circ\text{C}$ . The discrepancy between our results and these previous forced experiments could arise from the inability of the forced oceanic experiments to simulate adequately the likely positive ocean-atmosphere Bjerknes feedbacks. In the experiments described in this paper, the warming along the Kelvin wave path is associated with a weakening of the trade winds in the central-eastern Pacific that favours the growth of stronger SST anomalies. As shown in Figs. 9d and 12d, this reduction exceeds 20% between  $150^\circ$  and  $110^\circ\text{W}$  in April–May, and is a consequence of the decrease in the east-west SST gradient due to the initial central-eastern Pacific warming along the forced oceanic Kelvin wave path (Lengaigne et al. 2003a). This trade winds weakening induces an anomalous advection of heat by accelerating eastward surface currents. Moreover, it reduces the equatorial upwelling, limiting the amount of cold water brought to the surface. These processes further increase the initial SST anomaly.

Such coupled processes act to significantly amplify the SST signal associated with the forced oceanic response, resulting in this particularly intense warming of the central-eastern Pacific. This result is supported by observational studies that investigated the remote changes in SST following WWEs (Harrison and Giese 1989; Vecchi and Harrison 2000). Harrison and Giese (1989), who explored the remote response to a particular western Pacific WWE during May 1986, argue that this event was related to SST warming of over  $2^\circ\text{C}$  in July at the onset of the 1986/1987 El Niño. They underline the importance played by zonal and meridional heat advection in this warming, but did not investigate the

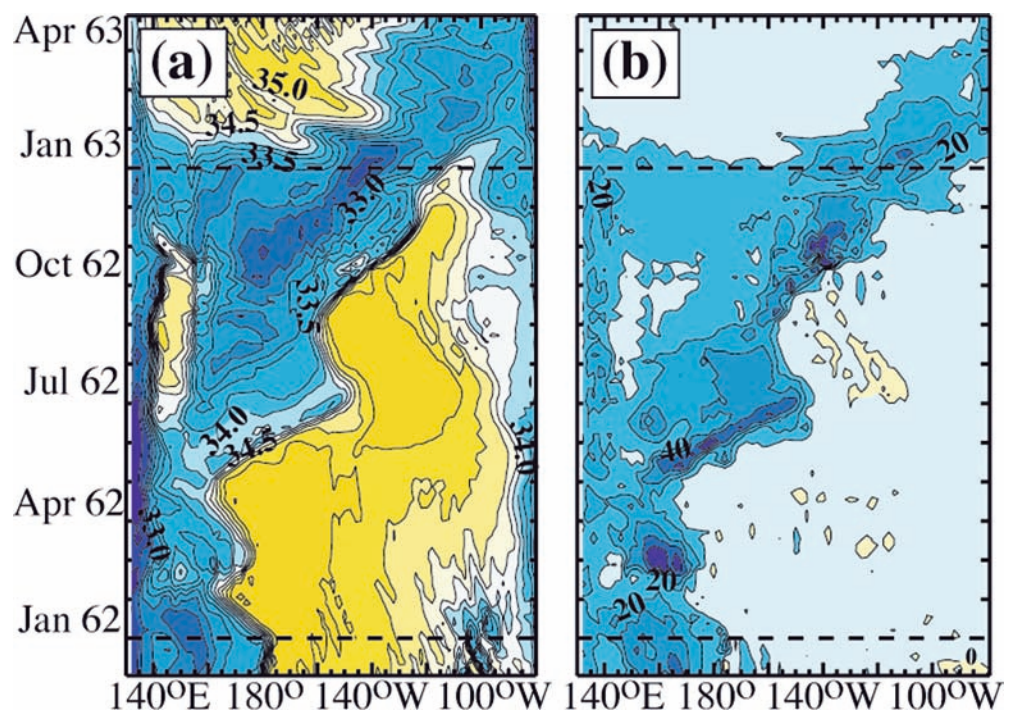
atmospheric variability during this time period. Vecchi and Harrison (2000) carried out a more systematic study of the remote SST changes following equatorial WWEs using a composite technique for the period 1986–1998. They argue that, when the tropical Pacific has near-normal eastern equatorial SSTs, equatorial WWEs are followed by substantial equatorial waveguide warming in the central/eastern Pacific (composite warming as large as  $1^{\circ}\text{C}$  80 days after the event) and that there is greater than 50% chance of moderate ( $>0.5^{\circ}\text{C}$ ) Niño 3 warming 60 days after strong WWEs, a result that is not in quantitative agreement with all the previous forced oceanic studies. In contrast, our model results are consistent with these observational findings: over the ten CWWE ensemble members, five display an SST warming that exceeds  $0.5^{\circ}\text{C}$  2 months after the inserted WWE (i.e. in April; Fig. 7). These large SST responses in the observational studies and the present coupled study are likely to be the result of the positive ocean-atmosphere interactions that are not represented in the forced experiments. However, it could also be argued that this strong model response could arise from a too strong sensitivity of the atmospheric model to SST anomalies. Further investigations of the remote changes in SST and zonal wind stress following WWEs are needed in both observations and coupled GCMs to draw definitive conclusions on this key issue.

The second strong impact of WWEs on the coupled system occurs at the EEWP where WWEs in the SW cases generate surface jets that efficiently advect warm waters eastward. It is worth noting that the rapid EEWP displacement that occurs following the inserted WWE for all the strong warm cases (red curves Fig. 9) is characterised by a large subsequent WWE activity

(Table 2) and long-lasting surface jets at the EEWP. Their duration varies from 1 to 2 months and their intensity from  $0.7$  to  $1.6\text{ m s}^{-1}$ . This WWE activity and accompanying long-lasting eastward jets are thought to be important features of the development phase of El Niño, and could contribute significantly to its intensity. In fact, these jets are a major factor in the advection of the warm pool eastward and therefore to the generation of positive (i.e. westerly) zonal wind stress anomalies in the central Pacific. They occur preferentially in a period when the seasonal trade winds reinforce and could therefore be key ingredients in preventing the return of warm waters back to the western boundary, as is usually the case in the seasonal cycle. In fact, the weak WWE activity in the MW case prevents the development of such jets (Table 2) and is characterized by a rapid westwards shift of the warm pool as the trade winds reinforce in July (Fig. 8a).

The mechanism that generates the intense surface jet in the SW case is complex. This jet is not a direct local response to the WWEs occurring from May to June since it is not collocated with the maximum WWEs (Figs. 9c and 10b), but develops to east of them. As shown in Fig. 16a, this jet is concomitant with the displacement of the sea surface salinity (SSS) front. This eastward moving jet results from a mechanism that is fully non-linear and has already been identified in forced mode (Boullanger et al. 2001; Lengaigne et al. 2002). In early May, the occurrence of a WWE in the western Pacific generates a geostrophic zonal current associated with the Kelvin wave that tightens and displaces the salinity front eastward (Fig. 16a). This eastward displacement is then amplified by the pressure gradient associated with the tightened salinity front. This current

**Fig. 16** Time longitude evolution for SW experiment averaged between  $2^{\circ}\text{N}$  and  $2^{\circ}\text{S}$  for sea surface salinity (SSS) (a), barrier layer thickness (BLT) (b). The contour interval is  $0.25\text{ psu}$  for salinity and  $10\text{ m}$  for BLT





intensification just at the EEWP results in a strong negative zonal gradient of surface currents at this location, allowing the momentum zonal advection terms to develop. This non-linear acceleration contributes strongly to the intensity and persistence of the zonal current front at the EEWP. In addition to these oceanic non-linear processes, other positive coupled feedbacks act to maintain this long-lasting zonal current front. The eastward advection of warm waters by this jet consequently displaces the atmospheric convective activity and intermittent positive winds therefore develop near the EEWP, which prolong the lifetime of the eastward jet (Fig. 9c). The vertical salinity structure also plays a key role to prolong the existence of the jet (Maes et al. 2002). As shown in Fig. 16b, the barrier layer thickness (BLT), defined as difference between the bottom of the isothermal layer and the bottom of the mixed layer, is very strong along the EEWP during 2 months associated with the intense surface jet. While the WWE that occurs in early May locally reduces the BLT in the region of the forcing, it favours the formation and growth of a deep barrier layer at the EEWP (Vialard and Delecluse 1998). In fact, the vertically sheared horizontal flow generated by this WWE at the eastern edge of the warm-pool advects the horizontal salinity gradient within the isothermal surface layers. This causes near-vertical salinity contours to tilt into the horizontal, thus generating a shallow halocline above the top of the thermocline. This barrier layer, by trapping the zonal momentum input into the ocean upper layer, acts to intensify the surface eastward jet at the EEWP. Moreover, the concomitant displacement of convection with the SSS front (Fig. 9c) acts to prolong the lifetime of this barrier layer with strong precipitation associated with convective events generating fresh water lenses just west of the EEWP.

The simulated jet during the El Niño development phase in the SW case is comparable to one that developed during the 1997/1998 El Niño. Figure 17 shows a vertical section of zonal currents at 170°W for SW experiment and TAO buoy measurements (McPhaden et al. 1998). Strong eastward jets trapped in the upper ocean layers occur in both model and observations from June to August (between 0.7 and 1.2 m s<sup>-1</sup> down to 50-m depth). The relatively moderate positive winds observed in the western Pacific during this time period in the observations (Fig. 11c) cannot alone explain the so particularly strong and long-lasting surface jets. Their intensity, as well as the strong zonal current shear in the surface layers, indicates that a mechanism similar to the one described above for the coupled model could be at work in the central Pacific during the 1997/1998 El Niño. Unfortunately, the lack of direct salinity measurements at depth during this period does not allow definite conclusions to be drawn. However, indirect barrier layer depth estimates by Maes (2000) suggest the existence of a strong barrier layer in mid-1997.

Similar intense surface jets have already been noticed in previous observational and modelling studies. Harrison and Craig (1993) reported the existence of such

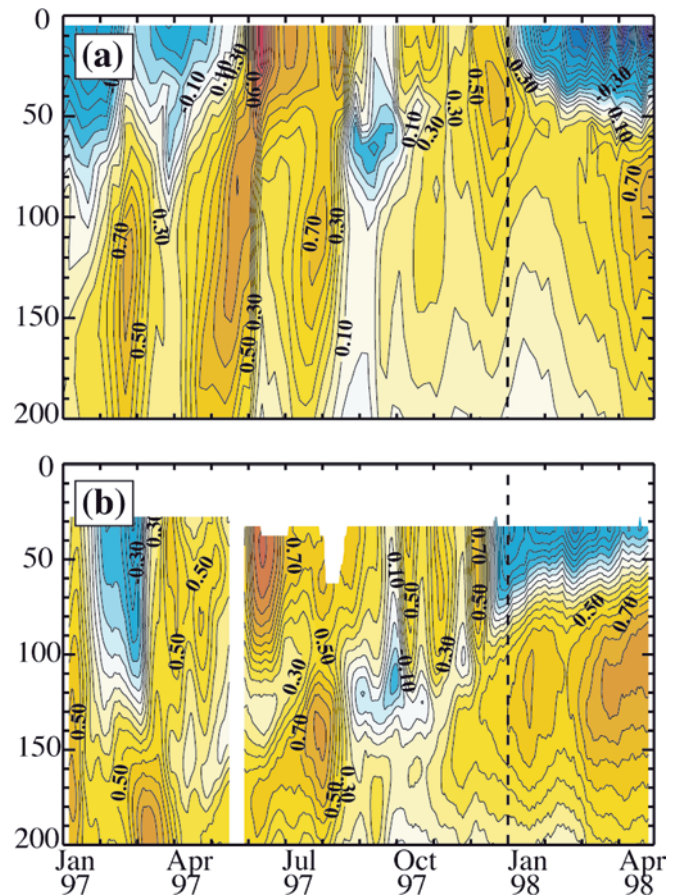


Fig. 17 Time evolution of 5-day mean zonal velocity profiles at 0°, 170°W for SW experiment (a), and TAO mooring (b). Contour interval is 0.1 m s<sup>-1</sup>

strong surface jets during November–December 1982 and in early 1983. Through the use of a primitive equation ocean model, they underlined the important contribution of zonal momentum advection in the formation of the jets and their impact on the temperature changes. Similarly, Harrison et al. (2000) pointed out the strong contribution of zonal momentum as well as zonal pressure gradient in the formation and duration of the intense jets (up to 1.2 m s<sup>-1</sup>) that were observed during November 1991–January 1992. Finally, Boulanger et al. (2001) and Lengaigne et al. (2002) suggested that the formation of a similar surface jet in early 1997 could be responsible for the extremely steep rise in the central Pacific SST. All these jets were found during El Niño events (1982/1983, 1991/1992 and 1997/1998) indicating that strong eastward surface flows are likely to contribute to the maintenance and/or progression of warm waters in the central Pacific as in the SW cases of CWWE ensemble.

## 6 Discussion and conclusion

In this study, a coupled ocean-atmosphere general circulation model with a reasonable mean climate and

seasonal cycle has been used to investigate the response of the coupled ocean-atmosphere system to a WWE over the equatorial Pacific. The results have demonstrated that a single strong WWE is capable of establishing the conditions required to trigger a strong El Niño event when the oceanic conditions in the tropical Pacific are favourable to the development of a warm event. The insertion of the WWE affects the coupled system in two ways. It generates a strong wind-forced downwelling Kelvin wave that propagates eastward generating intense SST anomalies in the central-eastern Pacific (up to 2°C 60 days after the inserted WWE), through a coupled ocean-atmosphere interaction that amplifies the initial warming associated with the oceanic Kelvin wave. This initial central-eastern Pacific warming decreases the east-west SST gradient, resulting in a weakening of the trade winds and a reduction in equatorial upwelling, both of which further increase the initial SST anomaly.

The WWE also initiates an eastward displacement of the warm-pool that induces an eastward shift of convection and promotes the occurrence of subsequent WWEs in the following months (Lengaigne et al. 2003a). These events reinforce the initial eastern Pacific warming through the generation of additional Kelvin waves. Moreover, they generate intense and long-lasting surface trapped jets at the eastern edge of the warm and fresh pool that act to further shift the warm waters eastward. The development and maintenance of these jets are associated with complex mechanisms. They are substantially affected by remote and local wind forcing, advection of zonal momentum, and the zonal pressure gradients related to the salinity front and the barrier layer created at the eastern edge of the warm pool. These surface jets are likely to be important features of the El Niño development phase since they counter the impact of the seasonal reinforcement of the trade winds in summer, which tends to shift warm waters back into the western Pacific from June–July. The simulated El Niño reproduces fairly well the main characteristics of the observed 1997/1998 El Niño event (SST evolution, WWE and surface jets activity ...), giving confidence in the modelled processes.

The use of a ten-member ensemble reveals substantial differences in the coupled ocean-atmosphere response to a WWE. Whereas four members develop into strong El Niño warming (up to 3°C anomaly in the Niño 3 region at the end of the year) as described above, four others members displayed a moderate warming and two remained in neutral conditions. This diversity between the members appears to be due to the internal atmospheric variability during and following the inserted WWE. In the four moderate warm cases, the warm-pool is initially shifted eastward following the inserted WWE, but the subsequent weak WWE activity (when compared to the strong warming cases) prevents the development of intense surface jets. The seasonal strengthening of trade winds in June–July can therefore act to shift warm waters back into the western Pacific, reducing the central-eastern Pacific

warming. In the two neutral cases, an intensification of the trade winds at the time of the inserted WWE is suggested to prevent the development of the central-eastern Pacific warming and to inhibit the eastwards shift of the warm pool.

This strong sensitivity of the response of the coupled system to WWEs most likely affects the predictability of the tropical Pacific and of El Niño events. The onset of the simulated El Niño strongly depends on the atmospheric variability in the western Pacific, especially the WWE activity during late spring and summer. The occurrence of a very intense WWE in the early year favours a stronger subsequent WWE activity through an eastward displacement of warm waters in the following months, but does not seem to totally constrain it. The stochastic nature of the subsequent WWEs in the model limits the predictability and therefore participates to the ensemble spread. These results are consistent with the fact that a strong WWE is not always followed by an El Niño and could explain the current controversy on the influence of atmospheric intraseasonal activity on ENSO. On the one hand, there is only a weak, negative simultaneous correlation between the interannual variations in the MJO and ENSO in the observations (Slingo et al. 1999; Hendon et al. 1999) whilst modelling studies have suggested that the high frequency forcing is not related with the ENSO cycle in any obvious way (Zebiak 1989; Syu and Neelin 2000). On the other hand, it has been suggested that high frequency atmospheric weather events can play a leading role in the evolution and amplitude of El Niño events (Perigaud and Cassou 2000; Boulanger et al. 2003; Lengaigne et al. 2003a) and cause ENSO irregularity (e.g., Penland and Sardeshmukh 1995; Blanke et al. 1997; Kleeman and Moore 1997). Our results tend to support these latter ideas, but the diversity of coupled response to a WWE underlines the complex relationship that exists between high frequency forcing and the ENSO cycle.

It is however worth noting that the initial state of the ensemble experiments used in this study were favourable to the development of an El Niño event and that the response of the coupled system with a significant oceanic heat deficit along the equator is likely to be very different, as suggested by simple models experiments (Fedorov 2002). Further fully coupled experiments investigating the influence of the initial state on the coupled response to WWEs are therefore required to analyze the seasonal and inter-annual dependence of the coupled response to WWEs and to understand to what degree WWEs are fundamental to the ENSO phenomenon. Moreover, some systematic model biases (weaker than observed WWE activity in the western Pacific, weaker SST gradient in the central Pacific, larger ENSO amplitude, ...) could impact the results presented here and the stability regime of the coupled model used could influence the coupled response to WWEs. Further similar experiments using other coupled models are therefore also required to confirm the present results.

**Acknowledgments** The comments of the anonymous reviewers led to significant improvements in the manuscript. The authors are also grateful to Gurvan Madec and the OPA team, who developed the ocean model, and to the Hadley Center, who developed the atmospheric model. Matthieu Lengaigne gratefully acknowledge Bertrand Duchiron for its computation of the observational data and the comments of M. J. McPhaden and W. S. Kessler on an earlier version of the manuscript. This work was supported by the Programme National d'Etude du Climat (PNEDC). Computations were carried out at CSAR, Manchester and at the IDRIS/CNRS, Paris.

## Appendix 1

### The Mann–Whitney test

The Mann–Whitney test is a non-parametric procedure, which is powerful to test the hypothesis that two sample populations ( $X$  and  $Y$ ) have the same mean of distribution against the hypothesis that they differ. The test is derived by examining the probability distribution of a linear combination of the ranks of the population under the null hypothesis that all the values are sampled from the same continuous distribution.

The procedure ranks the population's values from smallest to largest, assigning the rank 1 to the smallest observation, 2 to the next largest, and so on up to rank  $n$ , the number of elements in the two populations. Then, the Mann–Whitney statistics for  $X$  and  $Y$  are defined as follows

$$U(X) = n_x n_y + n_x(n_x + 1)/2 - W_x$$

$$U(Y) = n_x n_y + n_y(n_y + 1)/2 - W_y$$

where  $n_x$  and  $n_y$  are the number of elements in  $X$  and  $Y$ , respectively, and  $W_x$  and  $W_y$  are the rank sums for  $X$  and  $Y$ . The test statistic  $Z$ , which closely follows a normal distribution for sample sizes exceeding ten elements, is defined as follows

$$Z = \frac{U(x) - (n_x n_y)/2}{\sqrt{(n_x n_y (n + 1))/12}}$$

When this probability level is sufficiently small, we reject the null hypothesis and conclude that the two sample populations do not come from the same distribution.

## References

- Belamari S, Redelsperger J-L, Pontaud M (2003) Dynamic role of a westerly wind burst in triggering an equatorial Pacific warm event. *J Climate* 16:1869–1890
- Bentamy A, Quilfen Y, Gohin F, Grima N, Lenaour M, Servain J (1996) Determination and validation of average wind fields from ERS-1 scatterometer measurements. *Global Atmosphere Ocean Syst* 4:1–29
- Blanke B, Delecluse P (1993) Variability of the tropical Atlantic ocean simulated by a general circulation model with two different mixed layer physics. *J Phys Oceanogr* 23:1363–1388
- Blanke B, Neelin JD, Gutzler D (1997) Estimating the effect of stochastic wind stress forcing on ENSO irregularity. *J Climate* 10:1473–1486
- Boulanger J-P, Menkes C (1999) Long equatorial wave reflection in the Pacific Ocean from TOPEX/POSEIDON data during the 1992–1998 period. *Clim Dyn* 15:205–225
- Boulanger J-P, Durand E, Duvel J-P, Menkes C, Delecluse P, Imbard M, Lengaigne M, Madec G, Masson S (2001) Role of non-linear oceanic processes in the response to westerly wind events: new implications for the 1997 El Niño onset. *Geophys Res Lett* 28:1603–1606. DOI: 10.1029/2000GL012364
- Boulanger J-P, Menkes C, Lengaigne M (2004) Role of high- and low-frequency winds and wave reflection in the onset, growth and termination of the 1997/98 El Niño. *Clim Dyn* 22:267–280. DOI: 10.1007/s00382-003-0383-8
- Braconnot P, Joussaume S, Marti O, de Noblet N (1999) Synergistic feedback from ocean and vegetation of the African monsoon response to mid-Holocene insolation. *Geophys Res Lett* 26:2481–2484. DOI: 10.1029/1999GL006047
- Collins M (2002) Climate Predictability on interannual to decadal time scales: the initial value problem. *Clim Dyn* 19:671–692
- Cronin MF, McPhaden MJ (1997) The upper ocean heat balance in the western equatorial Pacific warm pool during September–December 1992. *J Geophys Res* 102:8533–8553
- Fedorov AV (2002) The response of the coupled tropical ocean-atmosphere to westerly wind bursts. *Q J R Meteor Soc* 128:1–23
- Fedorov AV, Harper SL, Philander SG, Winter B, Wittenberg A (2003) How predictable is El Niño? *Bull Am Meteorol Soc* 84:911–919
- Friedlingstein P, Bopp L, Ciais P, Dufresne J-L, Fairhead L, LeTreut H, Monfray P, Orr J (2001) Positive feedback between future climate change and the carbon cycle. *Geophys Res Lett* 28:1543–1546
- Giese BS, Harrison DE (1991) Eastern equatorial Pacific response to three composite westerly wind types. *J Geophys Res* 96:3239–3248
- Gregory D, Rowntree PR (1990) A mass flux convection scheme with the representation of cloud ensemble characteristics and stability dependent closure. *Mon Wea Rev* 118:1483–1506
- Gregory D, Kershaw R, Inness PM (1997) Parametrisation of momentum transport by convection II: tests in single column and general circulation models. *Q J R Meteor Soc* 123:1153–1183
- Guilyardi E, Madec G, Terray L (2001) The role of lateral ocean physics in the upper ocean thermal balance of a coupled ocean-atmosphere GCM. *Clim Dyn* 13:149–165
- Guilyardi E, Delecluse P, Gualdi S, Navarra A (2003) Mechanisms for ENSO phase change in a coupled GCM. *J Climate* 16:1141–1158
- Guilyardi E, Gualdi S, Slingo J, Navarra A, Delecluse P, Cole J, Madec G, Roberts M, Latif M, Terray L (2004) Representing El Niño in present-day coupled ocean-atmosphere GCMs: the dominant role of the atmosphere. *J Clim* (in press)
- Harrison DE, Craig A (1993) Ocean model studies of upper ocean variability at (0°N, 160°W) during the 1982–1983 ENSO: local and remote forcing. *J Phys Oceanogr* 23:427–451
- Harrison DE, Giese BS (1989) Comment on “The response of the equatorial Pacific Ocean to a westerly wind burst in May 1986” by M. J. McPhaden et al. *J Geophys Res* 94:5024–5026
- Harrison DE, Vecchi GA (1997) Westerly wind events in the tropical Pacific, 1986–1995. *J Climate* 10:3131–3156
- Harrison DE, Vecchi GA, Weisberg RH (2000) Eastward surface jets in the central equatorial Pacific, November 1991–March 1992. *J Mar Res* 58:735–754
- Hendon HH, Zhang C, Glick JD (1999) Interannual variability of the Madden-Julian oscillation during austral summer. *J Climate* 12:2358–2550
- Inness PM, Slingo JM, Woolnough SJ, Neale RB, Pope VD (2001) Organization of tropical convection in a GCM with varying vertical resolution: implications for the simulation of the Madden-Julian oscillation. *Clim Dyn* 17:777–793
- Inness PM, Slingo JM, Guilyardi E, Cole J (2003) Simulation of the Madden-Julian oscillation in a coupled general circulation model II: the role of the basic state. *J Climate* 16:365–382

- Kessler WS (2002) Is ENSO a cycle or a series of events?. *Geophys Res Lett* 29:DOI 10.1029/2002GL015924
- Kessler WS, Kleeman R (2000) Rectification of the Madden-Julian oscillation into the ENSO cycle. *J Climate* 13:3560–3575
- Kessler WS, McPhaden MJ (1995) Oceanic equatorial waves and the 1991–1993 El Niño. *J Climate* 8:1757–1774
- Kleeman R, Moore AM (1997) A theory the limitation of ENSO predictability due to stochastic atmospheric transients. *J Atmos Sci* 54:753–767
- Knutson TR, Manabe S, Gu DF (1997) Simulated ENSO in a global coupled ocean-atmosphere model: multidecadal amplitude modulation and CO<sub>2</sub> sensitivity. *J Climate* 10:138–161
- Larkin NK, Harrison DE (2002) ENSO warm (El Niño) and cold (La Niña) event life cycles: ocean surface anomaly patterns, their symmetries, asymmetries and implications. *J Climate* 15:1118–1140
- Latif M, Biercamp J, von Storch H (1988) The response of a coupled ocean-atmosphere general circulation model to wind bursts. *J Atmos Sci* 45:964–979
- Lengaigne M, Boulanger J-P, Menkes C, Masson S, Madec G, Delecluse P (2002) Ocean response to the march 1997 westerly wind event. *J Geophys Res* 107:DOI 1029/2001JC000841
- Lengaigne M, Boulanger J-P, Menkes C, Madec G, Delecluse P, Guilyardi E, Slingo JM (2003a) The march 1997 westerly wind event and the onset of the 1997/98 El Niño: understanding the atmospheric response. *J Climate* 16:3330–22243
- Lengaigne M, Madec G, Menkes C, Alory G (2003b) The impact of isopycnal mixing on the tropical ocean circulation. *J Geophys Res* 108:3345. DOI 10.1029/2002JC001704
- Lengaigne M, Boulanger JP, Menkes C, Delecluse P, Slingo J (2004) Westerly wind events in the tropical Pacific and their influence on coupled ocean-atmosphere system: a review, in *Ocean-Atmosphere Interaction and Climate Variability*. AGU Geophys Monogr (in press)
- Liebmann B, Smith CA (1996) Description of a complete (interpolated) outgoing Longwave radiation dataset. *Bull Am Meteor Soc* 77:1275–1277
- Madden RA, Julian PR (1994) Observations of the 40–50-day tropical oscillation: a review. *Mon Wea Rev* 122:814–837
- Madec G, Delecluse P, Imbard M, Lévy C (1998) OPA 8.1 Ocean general circulation model reference manual. Note du Pôle de modélisation, Institut Pierre-Simon Laplace. No. 11, pp 91
- Maes C (2000) Salinity variability in the equatorial Pacific Ocean during the 1993–98 period. *Geophys Res Lett* 27:1659–1662
- Maes C, Picaud J, Belamari S (2002) Salinity barrier layer and onset of El Niño in a Pacific coupled model. *Geophys Res Lett* 29:DOI 10.1029/2002/GL016029
- Mantua NJ, Battisti DS (1994) Evidence for the delayed oscillator mechanism for ENSO: the observed “oceanic” Kelvin mode in the far western Pacific. *J Phys Oceanogr* 24:691–699
- McPhaden MJ et al (1998) The tropical ocean-global atmosphere observing system. *J Geophys Res* 103:14169–14240
- McPhaden MJ (2002) Mixed layer temperature balance on intraseasonal time scales in the equatorial Pacific Ocean. *J Climate* 15:2632–2647
- McPhaden MJ, Yu X (1999) Equatorial waves and the 1997–98 El Niño. *Geophys Res Lett* 26:2961–2964
- McPhaden MJ, Freitag HP, Hayes SP, Taft BA (1988) The response of the equatorial Pacific ocean to westerly wind burst in May 1986. *J Geophys Res* 93:10589–10603
- Meinen CS, McPhaden MJ (2000) Observations of warm water volume changes in the equatorial Pacific and their relationship to El Niño and La Niña. *J Clim* 13:3551–3559
- Moore AM, Kleeman R (2000) Stochastic forcing of ENSO by intraseasonal oscillation. *J Clim* 12:1199–1220
- Neelin JD, Battisti DS, Hirst AC, Jin FF, Wakata Y, Yamagata T, Zebiak SE (1998) ENSO theory. *J Geophys Res* 103:14261–14290
- Penland C, Sardeshmukh PD (1995) The optical growth of tropical sea surface temperature anomalies. *J Climate* 8:1999–2024
- Perigaud CM, Cassou C (2000) Importance of oceanic decadal trends and westerly wind bursts for forecasting El Niño. *Geophys Res Lett* 27:389–392
- Picaud J, Ioualalen M, Menkes C, Delcroix T, McPhaden MJ (1996) Mechanism of the zonal displacements of the Pacific warm pool: implications for ENSO. *Science* 274:1486–1489
- Pope VD, Gallani ML, Rowntree PR, Stratton RA (2000) The impact of new physical parametrizations in the Hadley Centre climate model-HadAM3. *Climate Dyn* 16:123–146
- Reynolds RW, Smith TM (1994) Improved global sea surface temperature analyses using optimum interpolation. *J Climate* 7:1195–1202
- Roulet G, Madec G (2000) Salt conservation, free surface and varying volume: a new formulation for Ocean GCMs. *J Geophys Res* 105:23927–23942
- Schneider EK, Zhu Z, Giese BS, Huang B, Kirtman BP, Shukla J, Carton JA (1997) Annual cycle and ENSO in a coupled ocean-atmosphere general circulation model. *Mon Wea Rev* 125:680–702
- Slingo JM, Rowell DP, Sperber KR, Nortley F (1999) On the predictability of the interannual behaviour of the Madden-Julian oscillation and its relationship with El Niño. *Q J R Meteor Soc* 125:583–609
- Spencer H, Slingo JM (2003) The simulation of peak and delayed ENSO teleconnections. *J Climate* 16:1757–1774
- Syu H-H, Neelin JD (2000) ENSO in a hybrid coupled model. Part I: sensitivity to physical parameterizations. *Clim Dyn* 16:19–34
- Thompson CJ, Battisti DS (2001) A linear stochastic dynamical model of ENSO. Part II: Analysis. *J Climate* 14:445–466
- Valke S, Terray L, Piacentini A (2000) The OASIS coupled user guide version 2.4, Technical Report TR/ CMGC/00-10, CERFACS
- Vecchi GA, Harrison DE (2000) Tropical Pacific sea surface temperature anomalies, El Niño, and equatorial westerly wind events. *J Climate* 13:1814–1830
- Vialard J, Delecluse P (1998) An OGCM study for the TOGA decade. Part II: barrier-layer formation and variability. *J Phys Oceanogr* 28:1089–1106
- Vialard J, Menkes C, Boulanger J-P, Delecluse P, Guilyardi E, McPhaden MJ, Madec G (2001) Oceanic mechanisms driving the SST during the 1997–1998 El Niño. *J Phys Oceanogr* 31:1649–1675
- Wyrtki K (1975) El Niño—the dynamical response of the equatorial Pacific Ocean to atmospheric forcing. *J Phys Oceanogr* 5:572–584
- Xie P, Arkin PA (1997) Global precipitation: a 17-year monthly analysis based on gauge observations, satellite estimates, and numerical model outputs. *Bull Amer Meteor Soc* 78:2539–2558
- Yu L, Rienecker MM (1998) Evidence of an extratropical atmospheric influence during the onset of the 1997–8 El Niño. *Geophys Res Lett* 25:3537–3540
- Zebiak SE (1989) On the 30–60 day oscillation and the prediction of El Niño. *J Climate* 2:1381–1387
- Zhang RH, Rothstein LM (2000) Role of off-equatorial subsurface anomalies in initiating the 1991–1992 El Niño as revealed by the NCEP ocean reanalysis data. *J Geophys Res* 105:6327–6339